Masters Thesis

A bioelectronic implant for wireless detection and treatment of disease

Michael Florea

Supervisors: Marc Folcher,

Prof. Martin Fussenegger

D-BSSE, ETH Zurich

September 2016

Summary

Among the various sensor systems, biological sensors are the most sensitive, and unlike any other sensor class, are capable of differentiating even between highly similar proteins and metabolites. The exquisite specificity of biosensors have been used to sense disease-specific biomarkers as well as toxins, drugs and other molecules. For some applications, cells can be engineered to act as *in vivo* biosensors, to produce a therapeutic output directly in response to sensed signal(s). In many cases however, it is necessary to transmit the sensed signal to the patient, in order to either analyse it or to alert the patient to seek comprehensive medical care. This requires conversion of the biological signal to an electrical signal and transmission of this signal outside the body.

Here we design a bioelectronic implant that converts biochemical signals to electrical signals, transmits them wirelessly to the user, and uses near-infrared light to control production of therapeutic proteins by genetically engineered cells. In order to achieve biological to electrical signal conversion, we use genetically engineered cellulase producing 'sentinel' designer cells, which activate a kill-switch type cellulase sensor within the implant in response to disease signals. For communication, we use a wirelessly-powered RFID chip that can receive wireless power and transmit a specific radio frequency when the sensor is activated. We show that this system can be activated in the presence of relevant concentrations of endogenous signals, cause a detectable change in electrical readout, and transmit the signal wirelessly to the user. Finally, to provide an immediate therapeutic response, we use 'therapeutic' cells that have been engineered to produce therapeutic proteins in response to near infrared light, and show that they can effectively be controlled by a miniature red light system embedded in the implant.

The implant could therefore be used to continuously monitor for the emergence of disease-specific biomarkers or other biochemical signals, alert the practician to their presence, and produce a protein based therapeutic with high temporal precision. It may therefore open up new avenues in biomedical research, and enable new possibilities in detecting and treating a range of chronic disease.

Contents

List of Tables

List of Figures

Abbreviations

ATP	Adenosine Tri-Phosphate
cAMP	cyclic Adenosine 3’ Monophosphate
FOI	Fold Of Induction
GPCR	G-Protein-Coupled Receptor
pA	poly-Adenylation domain
PKA	Protein Kinase AC
P_{min}	minimal promoter
$P_{IFN\text{-}\beta*}$	mutated IFN-β promoter
AMP	Adenosine monophosphate
BSA	Bovine serum albumin
c-di-GMP	Cyclic dimeric guanosine monophosphate
GMP	Guanosine monophosphate
GTP	Guanosine triphosphate
DGC	Diguanylate cyclase
DGCL	Diguanylate cyclase light chain
GFP	Green fluorescent protein
HEK	Human embryonic kidney
IFN	Interferon
IRES	Internal ribosomal entry site
IRF3	Interferon-regulatory factor 3
PDE	Phosphodiesterase
RFP	Red fluorescent protein
SEAP	Secreted alkaline phosphatase
STING	Stimulator of intereferon genes
TBK1	TANK-binding kinase 1
hTERT	Human telomerase reverse transcriptase
hMSC-hTERT	hTERT immortalized human mesenchymal stem cell

I Introduction

1.1 Cell-based biosensors

Proteins and other biomolecules are by far the most specific and sensitive tools for sensing diverse chemicals. They have been extensively used in different *ex vivo* analysis systems, such as immune-based detection systems (ELISA) and others. These systems capitalize on antibodies, specific enzymes or catalysts to carry out the sensing function. Recently, the list has been expanded to intracellular receptors and transcription factors as part cell-free transcription-translation systems (1). In contrast, cell-based biosensors use living cells to carry out and report the sensing function, and could in principle be used as the sensing part for a continuously-monitoring sensor. In these protein receptor based biosensors, bacterial or eukaryotic cells' transduction pathways are rewired to control a reporter system ultimately leading to the production of; a colorant, a fluorescent protein, light, change of pH, or other signals, which can be converted by a specific interface into an electrical signal. The integrated electrical signal can than be processed, quantified, and analysed digitally (Fig. 1.1). Until now, cell-based biosensors have mainly been used in *ex vivo* settings for applications ranging from detection of biological entities such as the parasite *Schistosoma mansoni* (2), to abiotic chemicals such as arsenic (3), environmental toxins (4), neurotoxic substances (5), and many others (4, 6). Although cell-based biosensors still offer an attracting option as *ex vivo* sensors, they are by far more promising as *in vivo* sensors. In an *in vivo* biosensor scenario the requirement of externally maintaining and feeding the biological sensing unit is not necessary. However, the realization of cell-based biosensors *in vivo* is associated with considerable technical difficulties, and until now, they have been mainly used as part of closed-loop negative feedback systems, where the sensory signal directly controls the therapeutic output of the cell (7–10). Instead, stand-alone use of cell-biosensors has been limited due to the difficulty of engineering a miniature and biocompatible cell-machine interface that converts biological signals to electrical signals. Furthermore, a standalone bio-electronic implant requires a wireless system to transmit the information externally to the user. In this work, we develop an electrical switch that integrates a biological signal by sensing the production of secreted cellulase. Designer cells can be thus programmed to secrete cellulase upon detection of a biological cue. The cellulase signal is detected by a cellulose-based sensor, and converted to an electrical signal, integrated by an RFID (radio-frequency identification) module. This module transmits the signal as a specific radio frequency, which can then be read wirelessly outside of the body by a specific receiver.

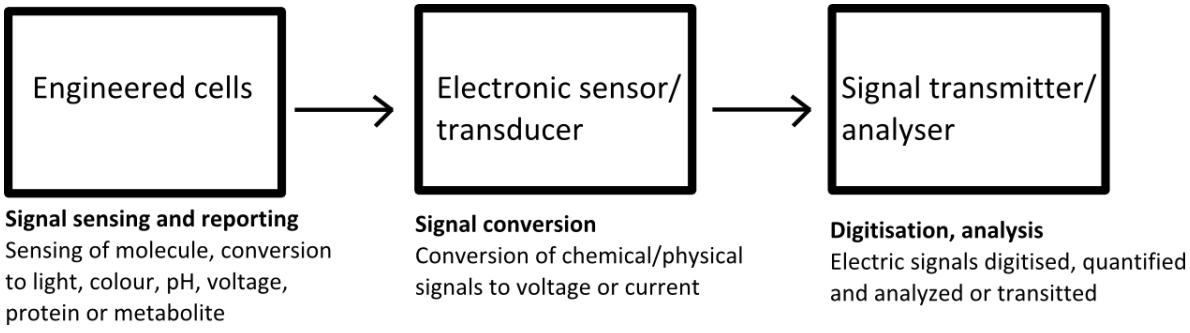

Figure 1.1 Schematic of a cell-based biosensor. Any cell-based biosensor consists of three modules: 1) engineered cells to sense the metabolite, and report it via a secondary signal, 2) an electronic sensor or transducer that converts this signal to current or voltage and 3) a unit, which digitises and analyses or transmits the signal for analysis.

1.2 Implants and implanted biosensors

With the exception of patient derived cells, use of cell-based sensors and therapies *in vivo* requires insulation of the implanted cells from the immune system, to prevent an adverse immune response. Until now, the majority of these efforts have used cells encapsulated in polymers, such as alginate, chitosan, agarose, PEG, PVE, cellulose and others (11–13). The past five years however has seen the development of macroscopic implants, where cells are insulated from the host via a porous, semi-permeable membrane (14–18). Compared to the use of polymer encapsulation, this confinement method has the advantages of being highly controllable and reproducible. It offers freedom of choice in quality-controlled materials for the membrane, as well as control over the pore size, the thickness of the cell layer and the scaffolding material. Adjusting these parameters allows better control over the rate of nutrient diffusion and minimizes necrosis of cells and immune activation of the host (14). Specifically, a high-capacity device was shown to induce vascularization and sustain cell viability and transgene

expression over several months (14, 17). These performances are associated with a flat-sheet design, a broad surface area, small cell chamber thickness (1-3mm), and relatively large pore size (450 nm), which allows for efficient diffusion of nutrients into the implant (14). Recent work has shown that near infrared light (NIR light) can be used to control gene expression in an implant *in vivo*, using wireless power delivery (16). Building on these results, here we use a minimized NIR gene expression control system, and combine it with a flat-sheet implant design for cell maintenance, which together allow for high-capacity cell maintenance with precise temporal control over gene expression.

1.3 Optogenetic gene expression control systems

Light based gene expression control systems allow highly detailed temporal control, and are readily electronically controllable (unlike chemical control systems) and do not result in potentially adverse effects on cells (unlike temperature and radio-frequency based control systems, which require either heating or cooling the cells). Multiple optogenetic signalling pathways have been developed, including those controlled by blue light (melanopsin, LOV-domain based, and cryptochrome-based sensors) (19, 20), red light (phytochrome-based sensors) (20, 21) and near-infrared light (bacterial phytochrome, and bacterial diguanylate cyclase based sensors) (16, 22, 23). In this work, we chose the latter for therapeutic gene expression control, since NIR light has the highest tissue penetration of the three, and is therefore most suitable for *in vivo* applications.

Specifically, we chose the bacterial diguanylate cyclase (DGCL)-based system, as it shows a large induction range of up to 50-fold, and was shown to function *in vivo* in genetically engineered human cells (16). The DGCL-based signalling pathway has been described in detail in Folcher *et al* (2014). Briefly, DGCL uses biliverdin as its chromophore, and changes from catalytically inactive to an active state upon illumination with 695 nm light (24). In its active state, DGCL catalyses conversion of GTP into cyclic-di-GMP (c-di-GMP), which acts as a second messenger to induce signalling through the STING pathway. Activation of STING leads to phosphorylation of interferon regulatory factor 3 (IRF3), which migrates into the nucleus and activates gene expression from type I interferon promoters (25). By linking a therapeutic gene to a type I intereferon promoter in an expression vector, it is therefore possible to control its expression through NIR light induction (16). In this work, secreted alkaline phosphatase SEAP (a commonly used reporter gene) was used in the place of therapeutic genes in order to ease the development and testing of the implant, however for therapeutic applications, it can modularly be replaced by a required therapeutic gene (see section 2.5 – Stable cell line engineering for more details).

1.4 G-protein coupled receptors as sensors for disease biomarkers

G-protein coupled receptors (GPCRs) are the largest class of mammalian cell-surface receptors. In humans, over 800 GPCRs have been identified, which act in a variety of functions, including sensing of taste, odorants, light, temperature, hormones, metabolites, small molecules and other signals (26–28). They are also pharmaceutically important, representing the targets of over half of all developed drugs (29). GPCRs consist of a 7-transmembrane domain, and associate with heterotrimeric G proteins. Upon ligand binding, conformation change in the protein leads to the exchange of a GDP to a GTP in the α subunit of the G-protein, which leads to dissociation of the G-protein complex from the GPCR, and the dissociation of Gα and Gβγ subunits from each-other (29). Different types of Gα then activate different downstream pathways (PKA pathway through cAMP signalling, NFAT pathway through Ca^{2+} signalling, or ROCK pathway through activation of Rho GEFs), leading to pathway-specific downstream gene expression (26–28).

In addition to traditional medicine, GPCRs have also found usage in synthetic biology, although majority of their applications are likely still emerging. In mammalian cells, melanopsins (blue-light sensitive GPCRs) have been used for optogenetic control of insulin production (19), rLHR (luteinizing hormone sensor) for bovine artificial insemination (11), cTAAR1 (a chimeric, drug inducible GPCR) for the treatment of metabolic syndrome (30) and CXCR2 (receptor for chemokine CXCL1 and CXCL8) for increasing the effectiveness of CAR T-cells (31, 32). In microbial systems, GPCRs have also been used to create medium-chain fatty acid sensors for metabolic engineering (33). Here, we take advantage of cTAAR1, induced by the hypertension drug Guanabenz, as an orthologous induction system for testing and developing the implant and the cellulase sensor (see *2.1 Cellulase sensor* below).

1.5 Cellulose and its degradation by cellulases

In order to developp a system to convert biochemical signals sensed by engineered cells into electrical signals, we develop a cellulase-based system, whereby cells sensing a biochemical signal produce cellulase, which leads to the degradation of a cellulose sheet and an associated change in electrical signal within in the implant.

Cellulose is chemically a polymer of β(1-4) linked D-glucose units, forms the main constituents of plant cell walls, and is estimated to be the most abundant biomolecule on earth (34, 35). Cellulases are a diverse class of enzymes capable of degrading cellulose to oligosaccharides or glucose monomers, and are produced by a variety of organisms, including bacteria, fungi, protozoans, and some animals (termites). Cellulases function by catalysing the hydrolysis of β(1-4) glycosidic linkages bonds between glucose monomers, and consist of 5 main classes:

- Endocellulases, which randomly cleave β (1-4) bonds within cellulose polymers
- Exocellulases, which cleave 2-4 units at the end of the cellulose polymer
- Cellobiases, which hydrolyse exocellulase products into monosaccharides
- Oxidative cellulases and cellulase phosphorylases, which depolymerase cellulase via oxygen radicals and phosphates respectively.

Here, we use cellulose due to its mechanical stability, strength and durability in the absence of degrading enzymes, and a secreted endocellulase previously engineered for rupturing cellulose encapsulating spheres (16). Since most animals, including humans, do not produce cellulases *in vivo*, implanted cellulose has been shown to be highly stable and also non-immunogenic (36). We take advantage of this property, to create a kill-switch type sensor system, where a cellulose sheet is stable and intact within the cellulase sensor, until a biochemical signal turns on cellulase production in engineered cells, leading to degradation of the cellulose sheet and sensor activation. Due to the stability of cellulose, this system allows for long-term monitoring of biochemical signal(s) within the patient, and minimization of false-positive activations.

1.6 Overview of the project

In summary, the purpose of this project was to engineer an advanced RFID-based medical bioelectronic implant that could be used to sense and wirelessly transmit information about the presence of biomarkers *in vivo*, and to produce a therapeutic output. To achieve this, the implant needed to fulfil the following requirements:

1) It must be small, strong, and biocompatible to be appropriate for human use.
2) It must be capable of supporting vascularization and high-density cell growth within the implant for an extended period of time.
3) It must be capable of sensing biochemical signals and converting them to electrical signals.
4) It must be capable of collecting wireless power and transmitting the signals wirelessly to the user, to alert the user to the presence of disease biomarkers.
5) It must be capable of allowing therapeutic gene expression of implanted cells, and enabling detailed temporal control.

In order to meet these requirements, we engineered an implant that houses a cell chamber containing genetically engineered mammalian cells and new systems to sense biomarkers and control therapeutic output (Fig 1.6.1). To sense disease biomarkers, we engineered a system comprising of a miniature, kill-switch type cellulase sensor integrated into the implant, and genetically engineered 'sentinel' cells, that express a user-defined GPCR complex to integrate circulating biomarkers and control the secretion of a recombinant cellulase. In this system, the occurrence of the targeted analyte leads to the production of cellulase by sentinel cells. It is the activation of the GPCR sensor (controlling the expression of cellulase) that converts the circulating biological marker signal into an electrical signal (Fig. 1.6.1). Specifically, we use the Guanabenz-inducible GPCR cTAAR1 within sentinel cells in order to develop and test the system, as Guanabenz is not found *in vivo* (thus reducing potential concerns about cross-reactivity and background-induced false positives), and cTAAR1 has been shown to be efficiently induced by Guanabenz *in vivo* (30) (Fig. 1.6.2). The signal is then integrated by an RFID chip, and transmitted as a specific frequency radiowave, allowing wireless transmission of the signal to the user. Finally, we use a wirelessly powered, miniaturized near-infrared light system embedded into the implant to control the gene expression of a 'therapeutic' cell line. This cell line houses therapeutic transgene(s) under control of a NIR light inducible pathway. In this pathway, bacterial diguanylate cyclase (DGCL) is induced by NIR light, and leads to the production and secretion of the therapeutic protein(s) through the STING pathway (Fig. 1.6.2). As result, this system can be used to externally monitor disease specific biomarkers, and to activate production of therapeutic proteins as a response.

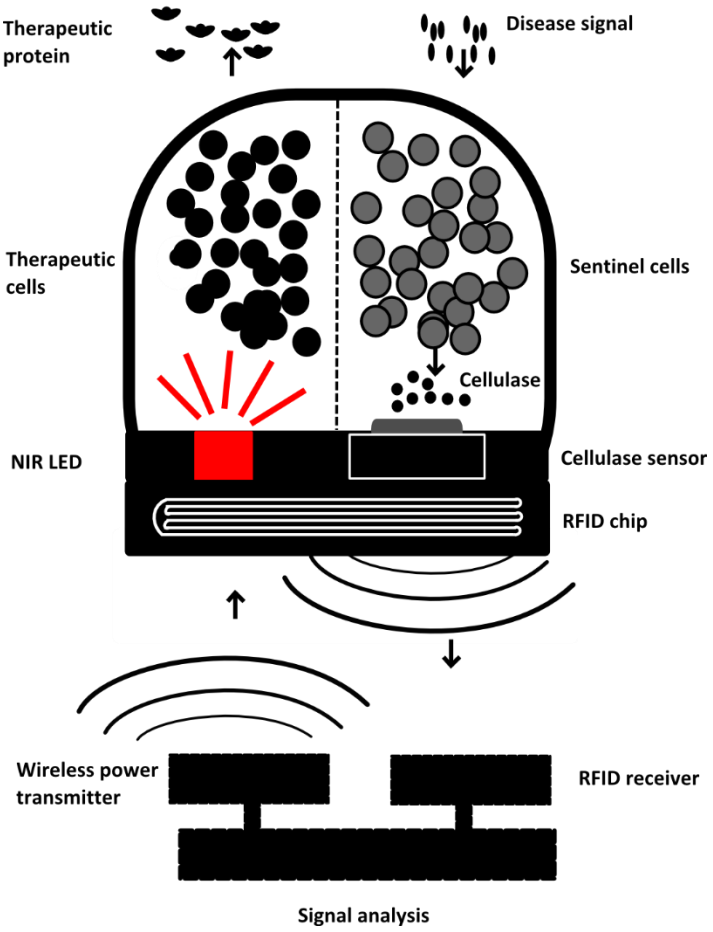

Figure 1.6.1. Overview of the RFID-based implant functioning. The implant contains engineered sentinel and therapeutic cells. The appearance of a disease biomarker or a signal induces sentinel cells to produce cellulose, which activates the cellulase sensor within the implant. The cellulase sensor state is read and transmitted by the RFID chip through 12 MHz –band radiowaves, which are detected by the RFID receiver. The signal is then analysed, and if warranted, the wireless power tranmitter activated to turn on the NIR LED light within the implant. The presence of red light then induces therapeutic gene expression and secretion from therapeutic cells.

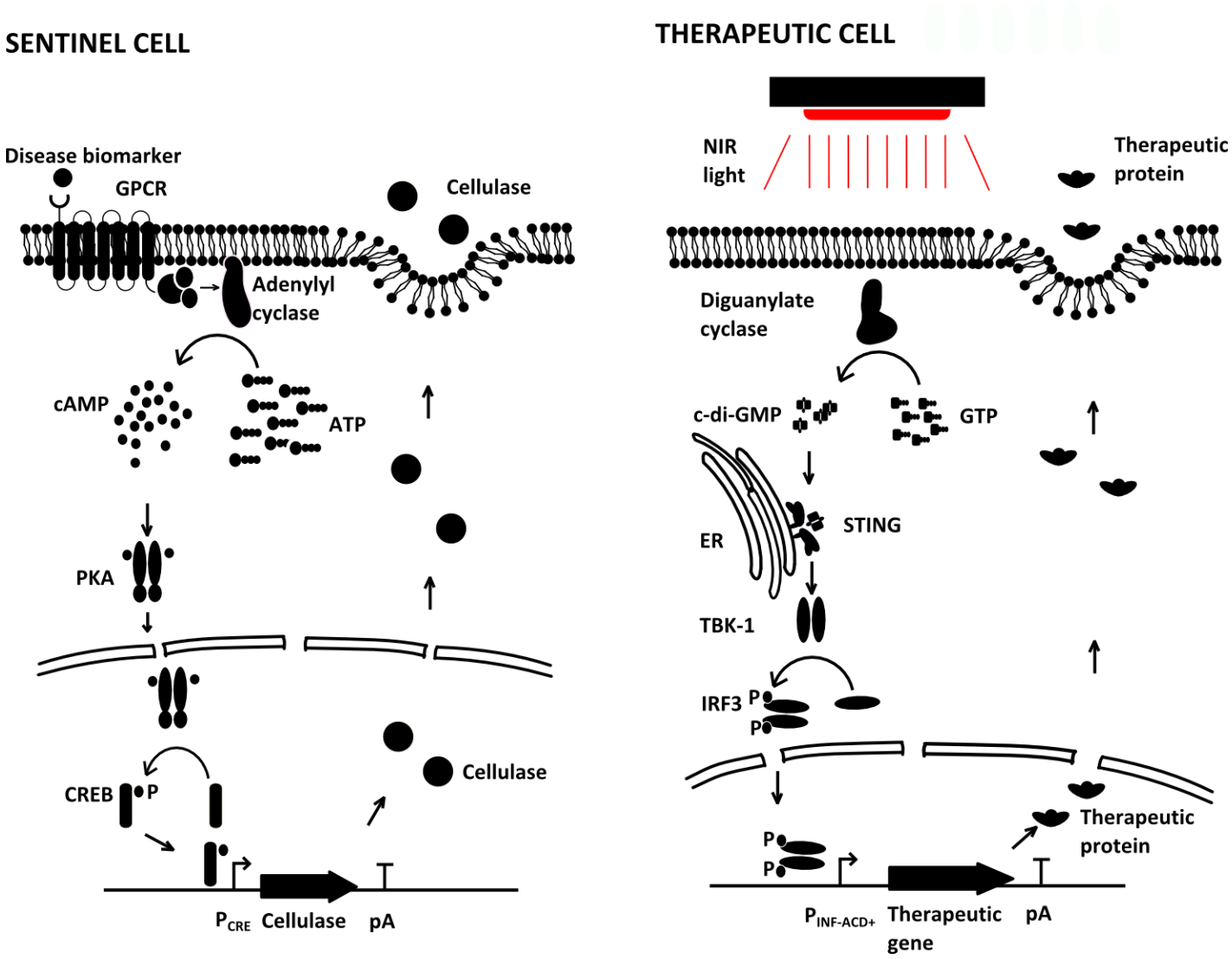

Figure 1.6.2. Overview of the geneticc circuits of sentinel and therapeutic cells. (Left) The sentinel cell genetic circcuit consists of cTAAR1, induced by Guanabenz. This activates adenylyll cyclase, which leads to increase in intracellular cAMP concentration, PKA-mediated phosphorylation of CREB, and production of cellulase from the P_{CRE} promoter. Cellulase is then secreted to activate the cellulose sensor. **(Right)** The therapeutic cell genetic circuit consists of a near-infrared light (NIR) inducible diguanylate cyclase, which catalyses c-di-GMP synthesis from GTP. Increased c-di-GMP concentration is sensed by ER-bound STING, which leads to tank-binding kinase 1 (TBK-1) activation, interferon regulatory factor 3 (IRF3) phosphorylation, and production of therapeutic proteins from P_{INF} promoter. Here, SEAP is used instead of therapeutic proteins, in order to ease the engineering and testing of the genetic circuit and the implant.

II Results and Discussion

2.1 Cellulase sensor

In order to transduce the biochemical signal, it was necessary to engineer a sensor that is capable of converting a biochemical signal into an electrical signal. As cellulase expression has been previously robustly linked to degradation of cellulose *in vivo* (37), the main goal of this section was to convert cellulose degradation into a measurable electrical signal. For this end, several different designs for a sensor were tested before a successful system was found. Below is the overview of this development.

2.1.1 Direct-current based cellulase sensor

Firstly, it was tested whether cellulose degradation in a cellulase test solution (consisting of cellulase in PBS solution, whereby PBS mimics the ionic strength and conductivity of human blood plasma) could cause a change in direct current (DC) resistance between two electrodes placed on either side of the membrane (Fig. 2.1.1 A). For this, tests were conducted where DC resistance across the cellulose sheet was measured, and resistances compared before and after artificially damaging the membrane. Several setups of cellulose membranes were used – a single sheet of cellulose, a single sheet of cellulose coated in mineral oil, and two sheets of cellulose with a thin sheet of mineral oil between sheets, to allow increased electrical insulation by mineral oil. When direct current was used, a change in resistance was observed before and after artificial damage, with the highest difference occurring for cellulose-oil-cellulose setup (Fig. 2.1.1 B-D). However, longer measurements in conductive solutions (PBS with and without cellulase) showed a steep change in resistance irrespective of whether or not cellulose sheets were present. This indicated that usage of DC causes electrochemical reactions on the surface of electrodes that considerably and quickly change the conductivity of the electrodes (Fig. 2.1.1 E-F). Electrochemical reactions cause cytotoxic by-products, strongly reduce electrode lifespan, and cause a change in conductivity which may mask any signals caused by degradation of cellulase, together making use of DC unsuitable for this purpose. Alternating current (AC) was therefore used for all further experiments.

2.1.2 Alternative-current based cellulase sensor

Next, alternative current (AC) was used in an improved setup, with electrodes placed on either side of a cellulose sheet in a conductive solution (Fig. 2.1.2 A), to determine whether this results in 1) removal of spontaneous electrochemical reactions on electrodes and 2) detection of cellulose degradation through change in conductivity. Different frequencies and voltages, ranging from 1 Hz to 1 kHz and 0.1 to $5V_{peak}$ (where V_{peak} denotes peak voltage of alternating current), and different wave-forms (sinusoid, rectangular) were used in the experiments. A frequency-dependent decrease in spontaneous resistance change was observed - in high frequencies, spontaneous change reduced to negligible levels (Fig. 2.1.2 B), while considerable change was observed with lower frequencies. No considerable changes were observed when different wave-form patterns were used (data not shown). This indicates that AC at sufficiently high frequencies minimises noise-generating electrochemical reactions on electrode surfaces. However, upon addition of cellulase, cellulose degradation resulted in no change in signal strength, despite complete sheet degradation (as determined by follow-up inspections) (Fig. 2.1.2 C). It is unclear as to why injury to the cellulose sheet could be detected with DC but not AC. However, a potential explanation may reside in the high electrical capacitance of the conductive solution. The conductive solution surrounding the cellulose sheet effectively acts as a capacitor, and the circuit as a capacitively coupled circuit due to alternating current. This indicates that degradation of the cellulose sheet would have little impact on the overall resistance of the circuit, and would not be detectable, making this strategy unsuitable.

2.1.3 Cellulose-resistor based sensors

As a result, the strategy was redesigned to eliminate the need for electrical current through the surrounding solution. To do this, we designed a cellulose-metal resistor based design, whereby a thin metal resistor is printed onto cellulose sheets, with the purpose of allowing current across cellulose when the cellulose sheet is intact, but not allowing current across cellulose when the sheet is degraded by cellulases (Fig. 2.1.3 A). In this strategy, several designs were tested. Firstly, a 2 kΩ titanium/gold resistor was deposited onto cellulose without further modifications to the cellulose (made by Dr. Giovanni Salvatore, ETHZ). However, testing showed that this resulted in a highly fragile and sensitive circuit, as 5/6 initially produced circuits failed to operate before manipulation. Under microscopic examination, several microscopic breaks could be observed in the circuit, most likely caused by formation of sharp edges in cellulose during handling, indicating that a potential reason

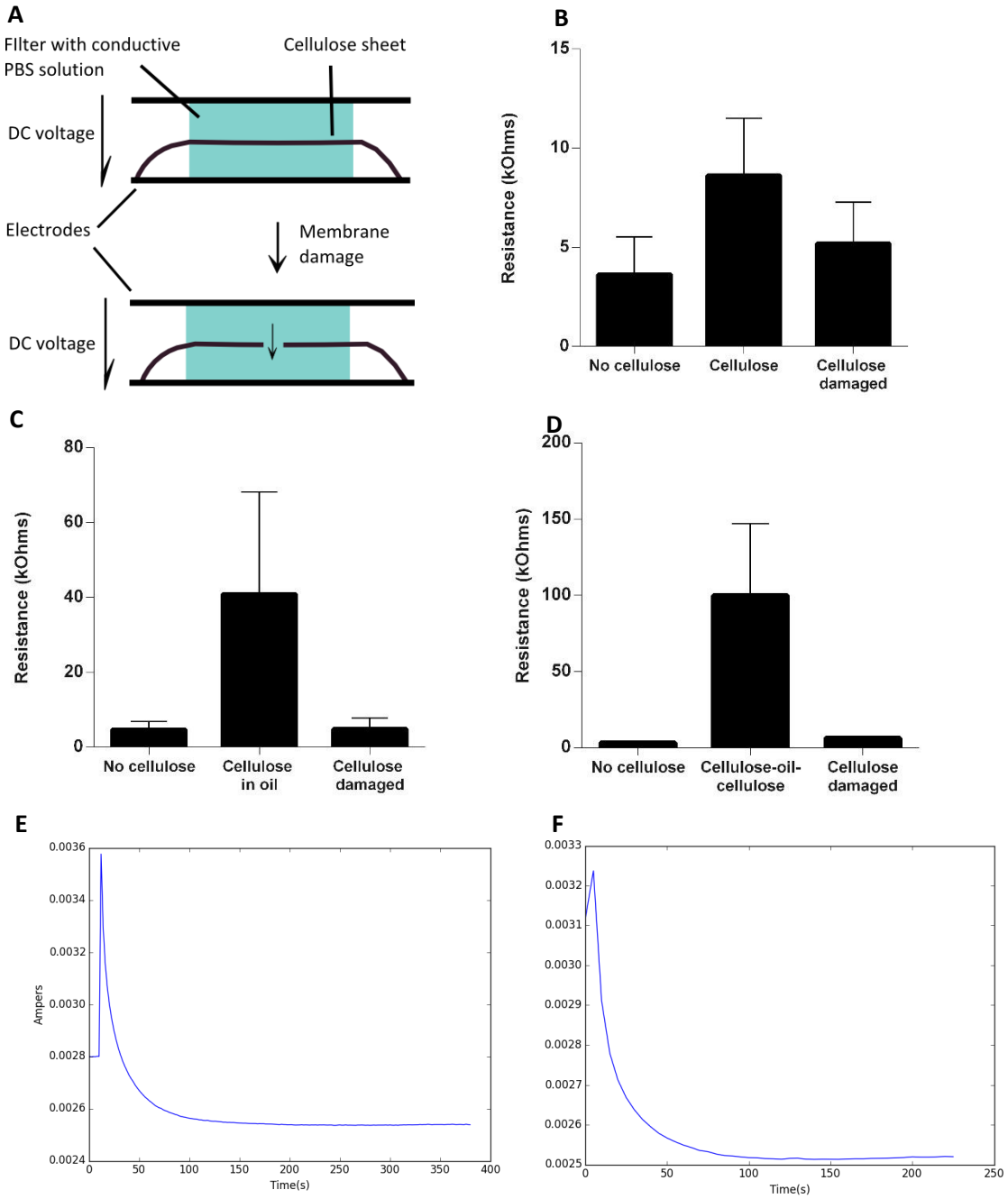

Figure 2.1.1. Direct current based cellulase sensor. (A) Set-up – a sheet of cellulose, cellulose with oil, or cellulose-oil-cellulose was placed in between filter papers containing conductive PBS solution, to provide contact with electrodes. Membrane was then artificially damaged and resistance measured before and after to determine whether this results in change in resistance **(B - D)**. Although resistance change was observed, long-term DC application on electrodes **(E-F)** caused spontaneous resistance change, indicating DC to be unsuitable for this application.

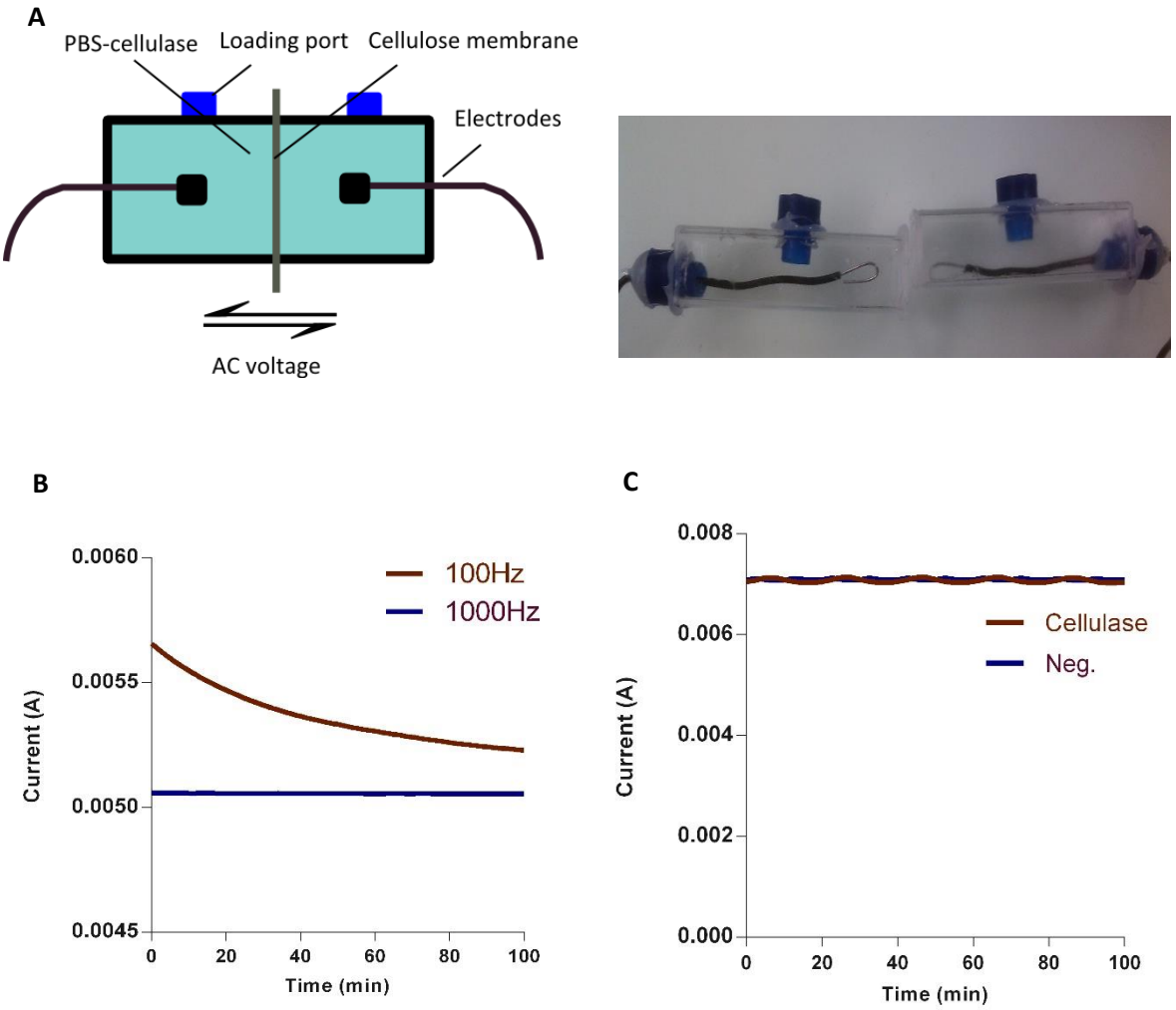

Figure 2.1.2 Alternative current for signal detection. (A) Overview of experimental setup – cellulose sheet was placed in conductive solution, between two electrodes, and AC voltage applied at different frequencies. **(B)** Effect of frequency on spontaneous electrochemical reactions causing resistance change (sinusoid waveform). High frequencies decrease spontaneous reaction rate to near negiglibe. **(C)** Effect of cellulose degradation on circuit resistance change. Unlike for DC, degradation of the cellulose membrane by cellulases resulted in no detectable change in signal readout.

for the failure of circuits was caused by poor attachment of the circuits to cellulose or microscopic damage caused by the sharp folding of the cellulose sheets (data not shown).

In the following tests, a thin sheet of insulating material, made of either of 200 nm thick PMMA (poly-methyl methacrylate) or 2 μm thick MAN1420 was therefore deposited between cellulose and the metal resistor, to allow a more robust attachment of the metal circuit to the underlying membrane and shield it from potential microscopic damage caused by sharp cellulose folding (Fig. 2.1.3 B). This circuit was wired using a carbon nanotube-based glue, and connected to NI myDaq and NI USB6008 data acquisition and control devices for generation and measurements of current. The functioning of the circuits were tested either in 1) fully immersed in cellulase-PBS solution or 2) a setup where only the cellulose part of the cellulose-insulator-metal circuit was exposed to a drop of cellulase or small amount of cellulase solution (Fig. 2.1.3 C). Despite several attempts, delicate handling and buffering against mechanical damage to protect the metal resistor, they failed to act consistently and produce robust and reproducible results when tested in cellulase-PBS solution (Fig. 3D). Microscopic observations and retests revealed several reasons for this:

1) During drying, conductive glue causes stresses on the cellulose surface, as it physically shrinks and visibly crumples the underlying cellulose membrane, which deforms and damages the resistor circuit. Furthermore, upon submersion to cellulase-PBS or any other liquid, the contact of the glue with cellulose can weaken to the point of visible de-attachment, at which point the mechanical stress is transmitted to the resistor, breaking it easily. No better alternatives for conductive glue are apparent however, as alternative wiring methods - clamping and soldering - immediately destroy the thin resistor layer.

2) Upon exposure to liquid, the cellulose sheet deforms, crumpling in a potato-chip like manner, which can deform and break the overlying resistor circuit.

3) Upon exposure to liquid, the contact between the resistor and underlying cellulose or insulating layer decreases, and in some cases results in the resistor visibly detaching from its substrate.

4) The insulating PMMA or MAN1420 layer is not efficiently removed by cellulase. Therefore, in the presence of small breaks in the insulating layer, the solution can access the printed resistor from the outset, while if no breaks are present, the resistor is not disturbed by cellulase.

In total, these observations indicated that this strategy was not appropriate due to the fragility of the deposited resistors, and the inherent trade-off between cellulase accessibility and circuit stability.

2.1.4 Cellulose-wire based sensors

Due to these considerations, it was clear that a more robust cellulose-circuit system would be required. As such, a different strategy was devised, whereby a thin, insulated copper wire was attached onto a small cellulose sheet and the wire-sheet system attached to a metal scaffold that subjects the cellulose-sheet to physical tension (Fig. 2.1.4 A). The idea behind this design was that the physical tension would mechanically break the cellulose sheet and the wire, only when cellulases degrade the cellulose sheet sufficiently to compromise its mechanical stability. Indeed, due to the robustness of the insulated wire, the system remained stable when submerged in PBS without cellulase (Fig. 2.1.4 B). However, when purified cellulase was added to PBS, degradation of cellulose led to weakening and ultimate breakage of the cellulose-wire system, generating a detectable signal change (Fig. 2.1.4 B). The breakage occurred both at high cellulase concentrations of 70 U/L, as well as cellulase concentrations of approximately 7U/L (Fig. 2.1.4 C), with the latter concentration being close to what can be produced by genetically engineered cells (see *2.3 Genetic engineering of cellulase production*). This indicated that when placed under appropriate tension, such cellulose-wire system may be degraded by cellulase producing cells, resulting in biological to electrical signal conversion.

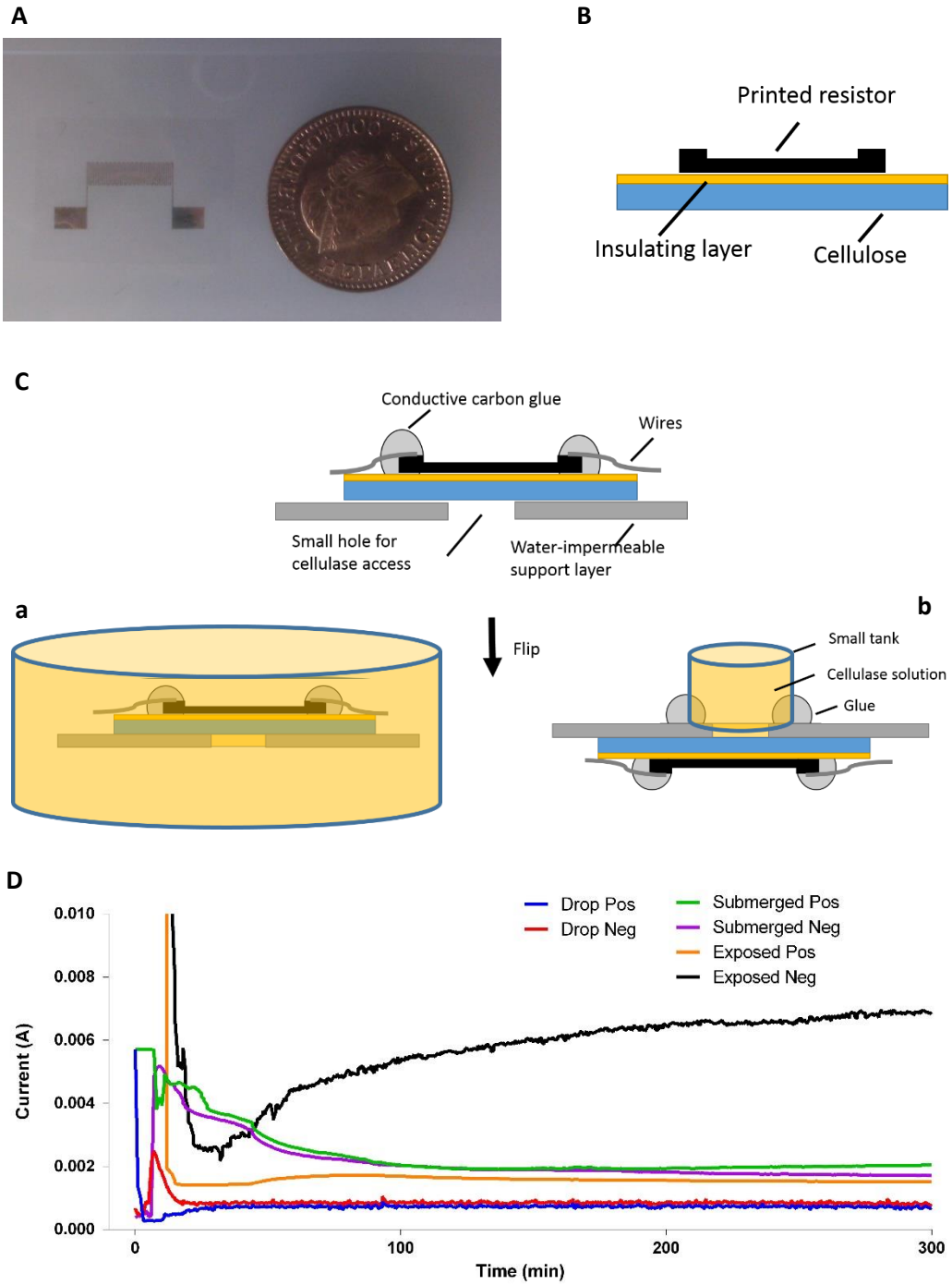

Figure 2.1.3 Using cellulose printed resistors. (A) Printed resistor. **(B)** Addition of extra insulating layers PMMA and MAN1420. **(C)** Experimental setup. Cellulose resistors were attached to a support layer and wired using conductive glue. Cellulose was then exposed to cellulase by either 1) pipetting a drop of cellulase onto cellulose (Drop), 2) submersion of the structure in cellulase completely (Ca - submerged) or exposing only the cellulose side to cellulase solution (Cb – exposed). **(D)** Representative graph of cellulose resistor behaviour when exposed to PBS-cellulase solution (PMMA covered). Similar results were observed with MAN1420-covered cellulase.

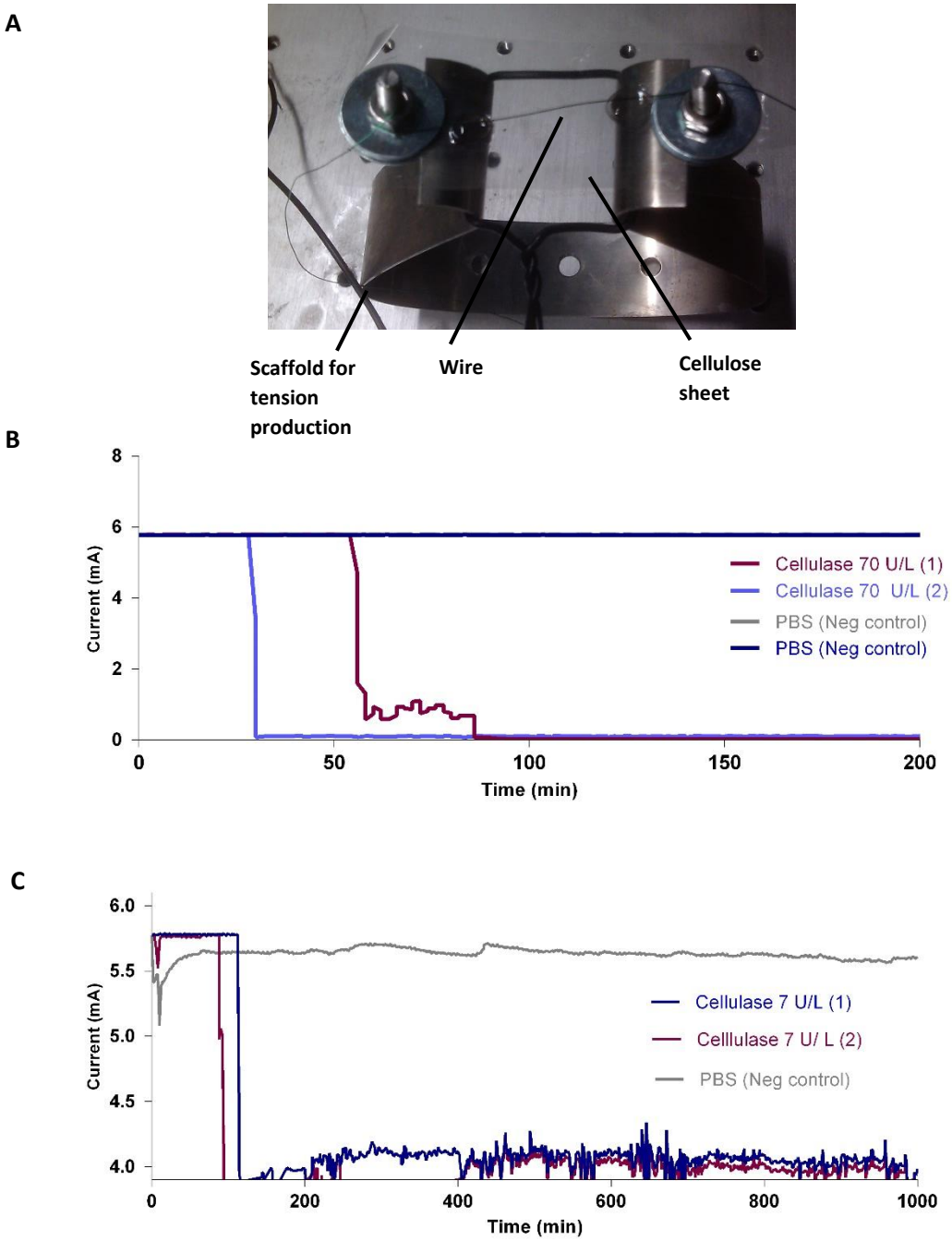

Figure 2.1.4 Cellulose-wire mechanism under stress. (A) Overview of the cellulose-wire mechanism. **(B)** Mechanism remains stable in PBS, but breaks after submersion into high-cellulase PBS solution (70U/L). **(C)** Similar results can be observed when lower concentrations of cellulase are used (7 U/lL) that are close to concentrations produced by transgenic cell lines.For Cellulase 2, fluctuations between 200 and 400 minutes were caused by transient lack of connection with the PBS solution after breaking. The OFF state of (C) remained at 4 mA instead of 0 mA, since in this setup, the broken wire remained in the conductive solution, instead of being exposed to non-conductive air.

In order to use this concept within an implant, it was however necessary to scale the size of the system to implantation-relevant dimensions. To achieve miniaturization, it was necessary to create a new miniature device to apply longitudinal tension to the cellulose-wire system. No pre-manufactured system that could be adapted for this purpose existed, necessitating a *de-novo* design of such a device.

For this purpose, several systems were designed, 3D printed and tested. They were based either on the supporting material itself or one or multiple small springs to generate the force necessary to strain the cellulose sheet (not shown). However, despite several re-designs and tests, this strategy could not be scaled down in a usable mechanism due to either:

1) The used materials (PLA, ABS) being too stiff to generate force,

2) The design being difficult or impossible to 3D print, or

3) The springs being unable to generate adequate force in the relevant sizes

2.1.5 Cellulose-switch based sensors

Due to the difficulties of producing a miniature-tensioning device, it was necessary to again redesign the strategy for the sensor. In order to remove the requirement for tension and moving parts, here, instead of using a wire, we used a miniature switch, which was mechanically closed (turned on) by a cellulose sheet, and would open (turn off) as a result of cellulose degradation. The goal behind this design was therefore, that a sheet of cellulose would be used to physically turn on the switch, and addition of cellulases would degrade the cellulose sheet, leading to opening of the switch and change in its electrical resistance. This design, still required some tension to turn on the switch, but this was considerably lower, allowing the use of non-moving and non-elastic parts.

In order to realize this design, 5 different microswitches were tested (see Table 7), with one (Omron B3U-3000P) showing the required characteristics of stability in saline solution and small size. It was therefore used for further experiments. Additional preliminary tests showed that a) a cellulose sheet could be used to turn on the Omron B3U-3000P microswitch, b) that addition of cellulase to the medium led to degradation and turning off of the switch, and c) that the changes in the state of the switch could efficiently be read out as electronic signals (not shown). Therefore this system was taken as basis for further development.

To build a system that would be suitable in a context of a small medical implant, it was necessary to design a device that would hold both the cellulose sheet and the switch, stress the cellulose enough to turn on the switch and enable cellulose to be accessible to the medium (in order to allow the cellulose sheet to be degraded by cellulase). Therefore, a device consisting of a miniature port to hold the switch, microscrews to hold the cellulose sheet, and microscrews to tension the switch was designed. The port to hold the cellulose was designed and 3D printed for prototyping first using PLA and ABS materials by the author, and when exceeding the resolution of available printers, ordered from Formlabs Standard resin, or polyamide PA 2200 from commercial vendors (see Table 7 for details). From the latter two, despite providing potentially higher resolution, Formlabs Standard resin was abandoned due to considerable cytotoxicity, whereby PA 2200 was both non-cytotoxic and high-resolution enough to meet the requirements of the design. Similarly, different microscrews, nuts and bolts were tested for size, operation and toxicity (not shown), and solid-brass microscrews were finally used. The device was continuously improved and minimized over design-build-test cycles to ultimately yield a system both functional and small enough to fit into a medical implant (Fig. 2.1.5.1).

In order to test the functionality of the cellulose-switch sensor, it was tested in PBS with or without different cellulase concentrations, and in culture supernatants of HEK 293T cells transfected with the cTAAR1- cellulase pathway (plasmids pKZy38 and pCK71, encoding for P_{min}-cTAAR1-pA and P_{CMV}-cellulase-pA respectively). In this pathway, the chimeric GPCR cTAAR1 is activated by the hypertension drug Guanabenz, and leads to cellulase production from P_{CRE} promoters (Fig. 1.6.2). Both tests showed that the cellulose-microswitch system can sense cellulase in a concentration-dependent manner and is not jammed or switched off by prolonged incubation in PBS or untransfected cell culture supernatants (Fig. 2.1.5.2). Note that the difference in times to signal activation between the two transfected HEK 293 T cultures may have been due to differences in cellulase production or sensor sensitivities (Fig. 2.1.5.2 B). This demonstrates that the miniature switch-based cellulose sensor can be used to sense levels of cellulase achievable by engineered cells, and convert the biochemical signal into an electrical signal.

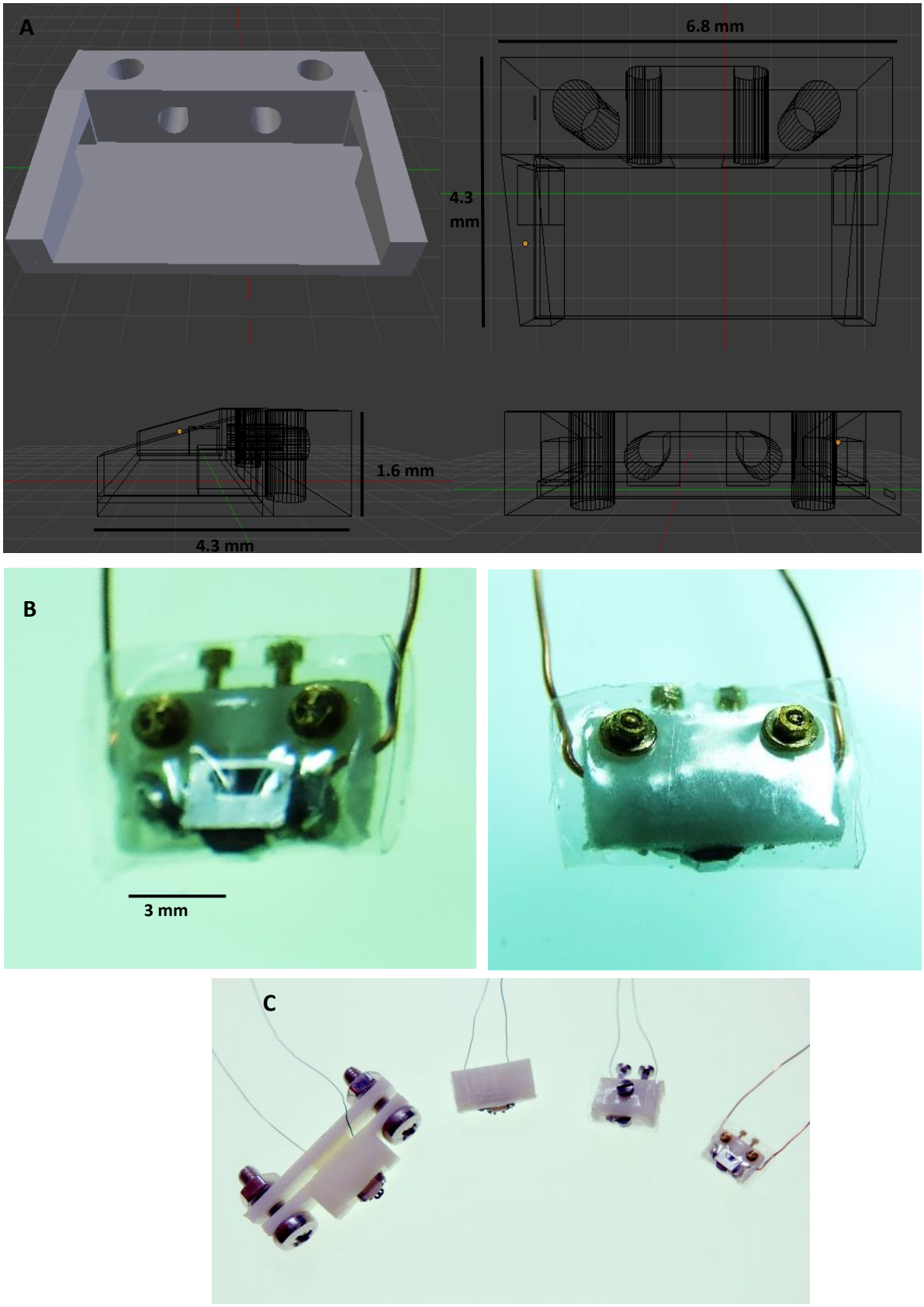

Figure 2.1.5.1 Microswitch-based cellulose sensor. (A) Design and overview of the final 3D printed microswitch port. **(B)** Assembled microswitch-cellulose sensor viewed from the top (left) and bottom (right). The microswitch is placed into the switch port and covered with 2 layers of cellulose membrane, which is attached to the port via microscrews, washers and nuts. Microscrews at the back of the port are then screwed and tensioned, to push the switch against the cellulose membrane and turn it on. **(C)** Previous designs of the microswitch-cellulose sensor, continuously minimized over design-build-test cycles.

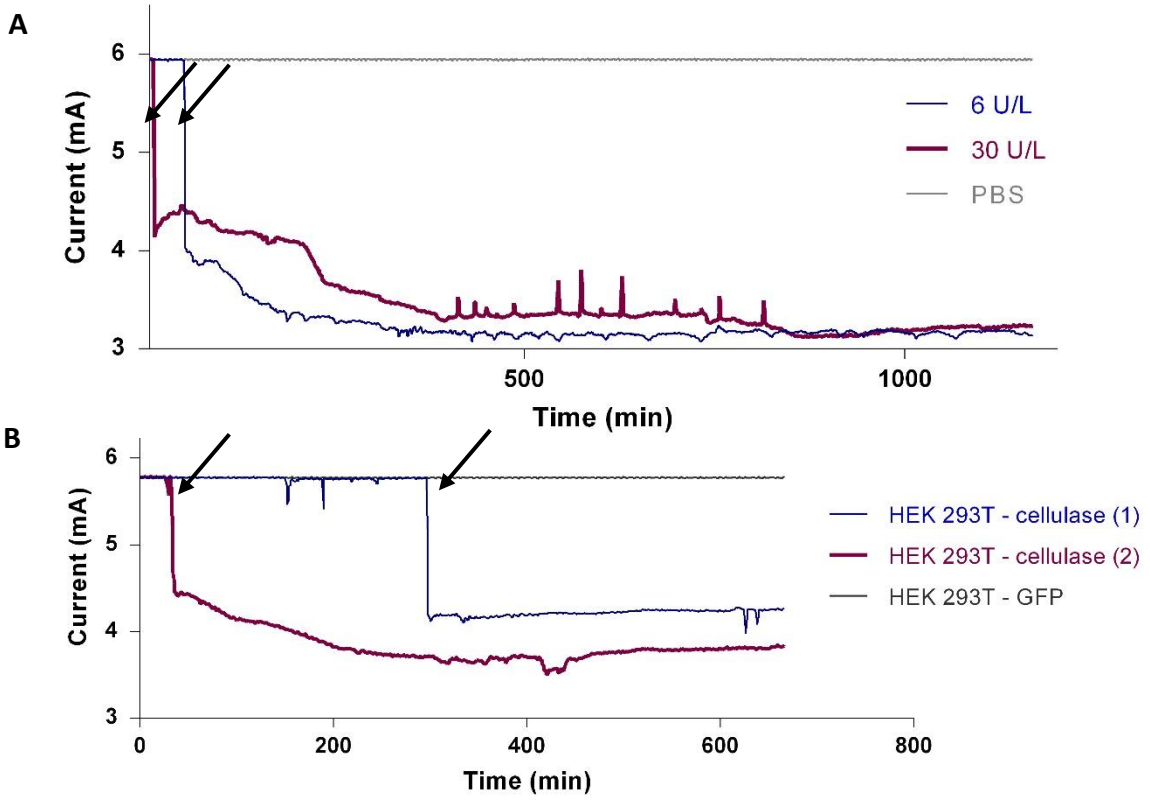

Figure 2.1.5.2 Testing of the microswitch-based cellulose sensor. (A-B) Functioning of the microswitch-sensor in cellulase-PBS and in cell extracts of HEK 293T transfected with either cellulase (two different transfections) or GFP. When the cellulose sheet is intact, the switch is closed (ON state), resulting in 6mA current. Addition of cellulase either in PBS solution or produced by cells results in the weakening of the cellulose membrane and the opening of the switch (OFF state), causing a rapid drop in current (marked by arrows). Furthermore, the switch remained in the ON state for at least 2 days in this experiment, and up to 5 days in other experiments (not shown), indicating that the cellulose sheet and the microswitch function relatively robustly in the absence of cellulase.

2.2 Modular GPCR-based circuits

Despite being successful as proof of principle, the tests with HEK 293T engineered to contain the cTAAR1-cellulase circuit (Fig. 2.1.5.2) indicated that several modifications to the pathway had to be engineered. Firstly, cells transfected with pCK71 but not induced for cellulase production showed considerable basal expression level, which was likely be sufficient to be activate the cellulose-switch device in the absence of a signal (Fig. 2.2.2.1 A). Secondly, multiple studies from previous authors have indicated that HEK 293T is not a suitable host cell line for long-term implantation (see below). It was therefore necessary to adapt the cTAAR1-cellulase circuit to a cell line suitable for long-term implantation, and also re-engineer it have a reduced leakiness, before it could be used within a medical implant.

Previous work has identified specific cell lines compatible with encapsulation process, including HEK 293T (30), HEK 293 Freestyle (16), C2C12 (15), ARPE19 (15, 38) and hMSCs (39). These cells have been successfully implanted into mice, rats or humans. From these lines, we selected hMSC-tert and ARPE19 as therapeutically relevant cell lines, as they do not suffer from the lack of contact inhibition or immunogenicity concerns. Although both hMSC and ARPE19 have been used in human clinical trials (18, 40), have associated cGMP production protocols (13, 41) and are suitable for long-term implantation, preliminary tests showed that transfection efficiencies of ARPE19 via PEI or Lipofectamine were very low (Fig. 2.2) making transient transfection and testing of circuits in ARPE19 practically difficult. Low transfection efficiencies for ARPE19 have also been reported elsewhere (42). Preliminary testing of genetic circuits using transiently transfected plasmids is critical for development of the circuits. Therefore, hMSC-tert was chosen as the main cell line for further experiments, with HEK 293T used as a secondary cell line for preliminary testing of circuits.

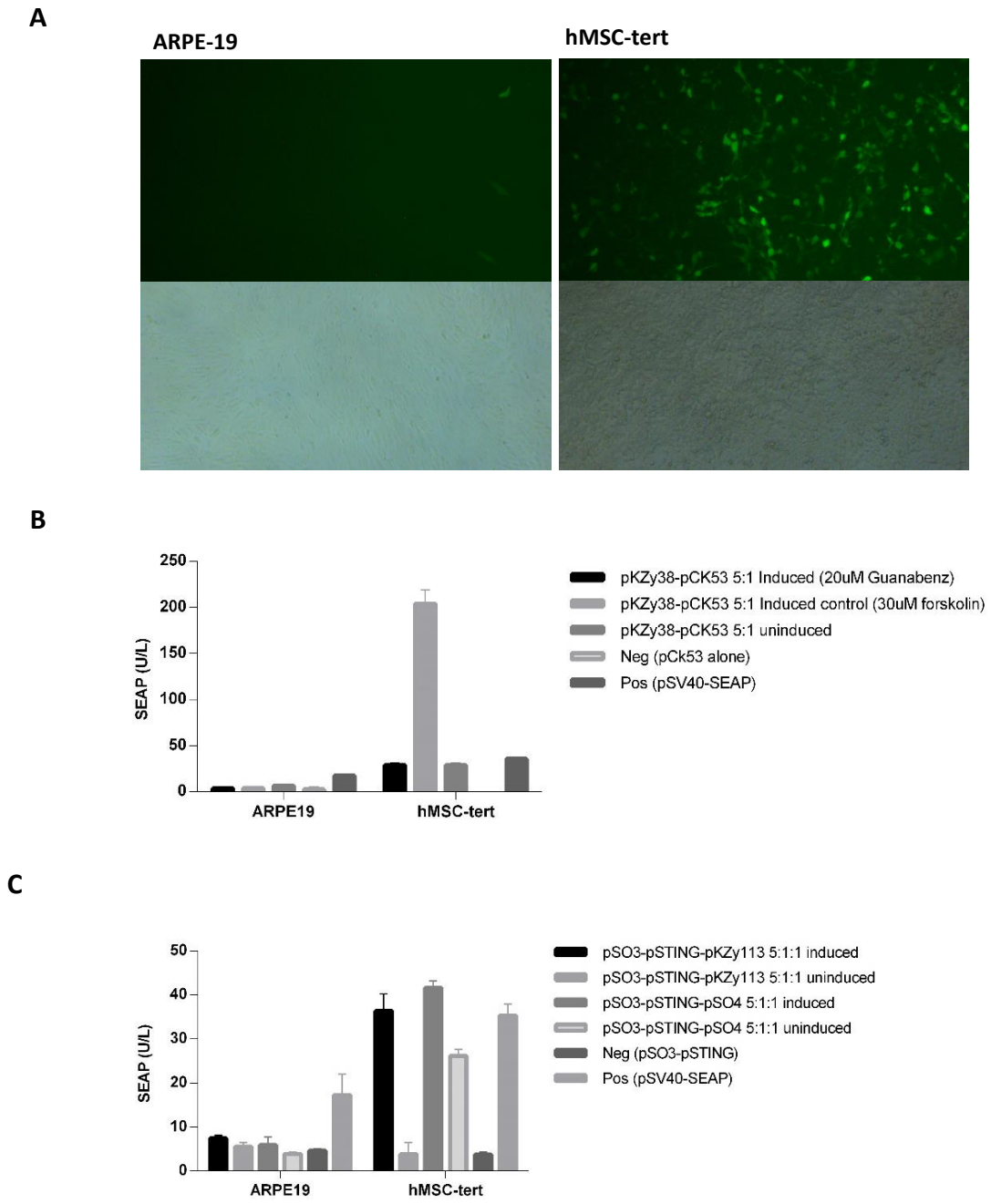

Figure 2.2 Comparison of transfection efficiencies of ARPE19 and hMSC-tert. (A) ARPE19 and hMSC-tert transfected with EGFP usng PEI (top panel – fluorescence microscopy, bottom panel – bright field). **(B)** Transfection of ARPE19 and hMSC-tert with pKZy38 and pCK53 at 5:1 ratios using Lipeofecsstamine 3000. Both induced with 20 µM Guanabenz or 30 µM forskolin and SEAP measured 48h later**. (C)** Transfection of ARPE19 and hMSC-tert with the Nir sensitive DGCL pathway using Lipofectamine 3000. Both were induced 16 hours after transfection with 700nm light under plate LEDs for 8 hours, and SEAP was quantified 48 h later. ARPE19 shows low transfection efficiencies both with PEI and Lipofectamine 3000, and shows no response to inducers when transfected either with cTAAR or DGCL pathways.

2.2.1 Guanabenz-inducible circuit in hMSC-tert

As hMSC-tert was chosen as the target cell line for clinical applications, it was necessary to re-engineer the Guanabenz-inducible cellulase circuit to be functional in hMSC-tert. Initial attempts showed that the circuit, consisting of plasmids pKZY38 and pCK71 operated well in HEK 293T, but not in hMSC (Fig. 2.2.1.1 A). Tests with forskolin induction (which trigger intracellular cAMP surge, causing signalling through the PKA pathway and activating the pCRE promoter controlling cellulase), showed that in hMSCs, cellulase could be effectively induced by forskolin, but not by Guanabenz (Fig. 2.2.1.1 A). This indicated that cTAAR1 expression from pKZY38 in hMSCs, unlike in HEK 293T was suboptimal. To test cTAAR1 expression driven from promoters of different strengths, pKZY38 derived cTAAR1 was subcloned under the transcriptional control of P_{SV40} (pMFl05, cloned by into pSAM200 backbone), P_{CMV} (pMFl06, cloned into pMM27 backbone) and $P_{EP1\alpha}$ (pMFl07, cloned into pMM28 backbone) and tested with pCK53, a plasmid encoding P_{CRE}-SEAP-pA. Additionally, cTAAR1 behind P_{SV40} promoter in a different plasmid (pKZy73) was tested. From the tests, cTAAR1 driven by P_{SV40} in pMFl05 showed best performance (Fig. 2.2.1.2 A). Further optimization of pMFl05:pCK53 ratios improved induction levels (Fig. 2.2.1.2 B). Finally, cTAAR1 was tested with co-transfection of Receptor-Transporting Protein 1 Short (RTP1S), a chaperone that facilitates trafficking and potentially also folding of functional odorant GPCR receptors (43, 44). Interestingly, co-transfection with pRTP1S at different ratios lead to decreased basal activity, and resulted in expression levels and induction ranges comparable to that of the cTAAR1 circuit within HEK 293T cells (Fig. 2.2.1.2). The exact mechanistic reason why RTP1S lead to improved fold induction is unclear, but improved cTAAR1 folding by pRTP1S, reducing background signalling, is a possible explanation.

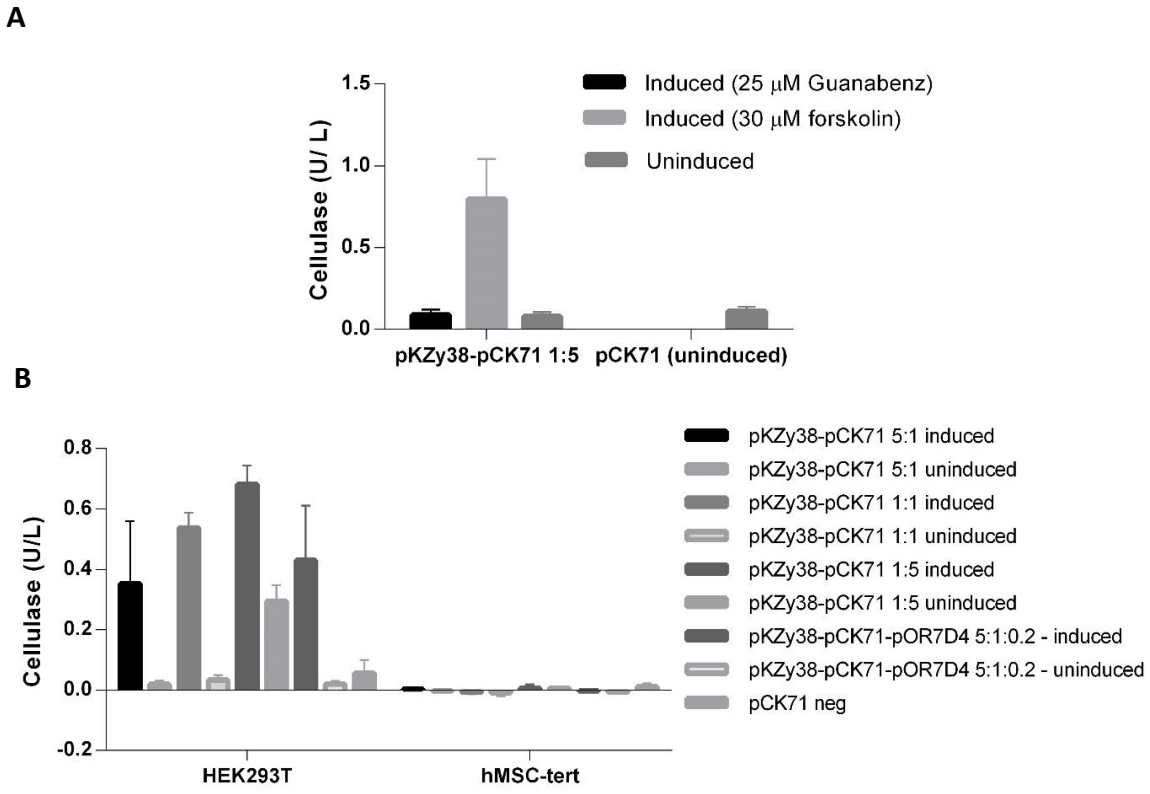

Figure 2.2.1.1 pKZy38 does not efficiently express cTAAR1 in hMSC-tert. (A) hMSC-tert transfected with pKZy38:pCK71 at 1:5 ratio, induced with 25 μM Guanabenz, and cellulase measured 48h post-induction. **(B)** HEK 293T and hMSC-tert transfected with various ratios of pKZy38-pCK71, induced with 100 μM Guanabenz, and cellulase measured 48h post-induction. hMSC-tert shows no induction at different ratios. As preliminary testing with forskolin induction led to efficient production of cellulase (B), these results indicated that unlike in HEK 293T cells, cTAAR1 is not efficiently produced from the plasmd pKZy38 in hMSC-tert.

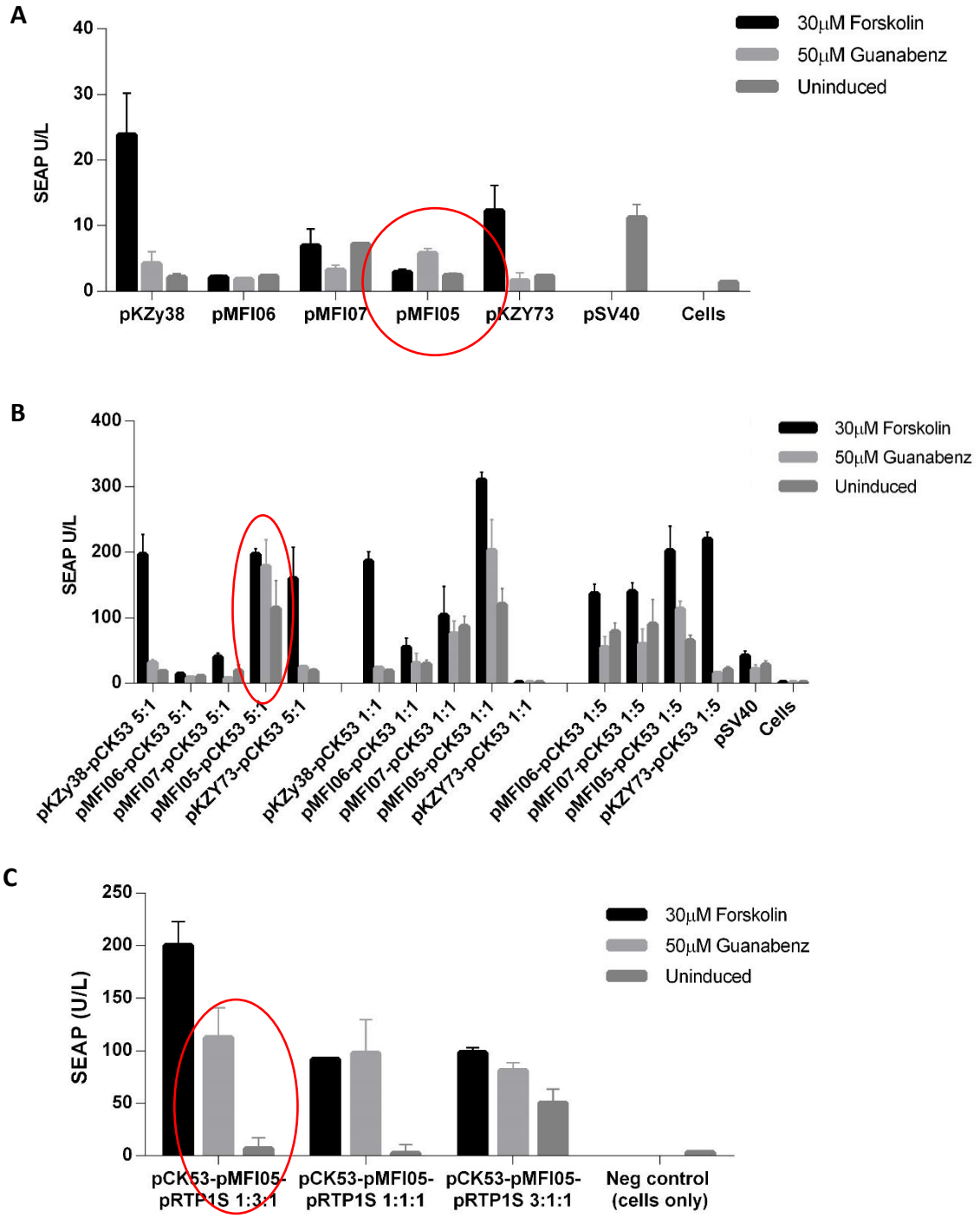

Figure 2.2.1.2 Re-engineering cTAAR1 expression vectors for hMSC-tert compatibility. (A) hMSC-tert transfected with pCK53 (SEAP reporter) and with pKZy38, pKZy73 (pSV40-cTAAR1-pA), pMFI05 (pSV40-cTAAR1-pA), pMFI06 (pCMV-cTAAR1-pA) or pMFI07 (pEP1α-cTAAR1-pA) at 5:1 ratio. **(B)** hMSC-tert transfected with the same plasmids at different ratios. Of the 5 plasmids, pMFI05 showed best induction (red circles), and was chosen for further studies. **(C)** hMSC-tert transfected with pCK53, pMFI05 and pRTP1S at different ratios. pRTP1S co-transfection dramatically reduces leakiness, and of the three ratios, 1:3:1 provides best results. Therefore, by expressing cTAAR1 from pMFI05 and co-transfecting with pRTP1S, it is possible to achieve high induction by Guanabenz in hMSC-tert. In all experiments, cells were induced with 100 μM Guanabenz or 30μM forskolin, and SEAP was measured 48h post-induction

2.2.2 Reducing leakiness of cellulase expression

Preliminary tests with pCK71 (P_{CMV}-cellulase-pA) showed considerable basal expression of both uninduced HEK 293T cells (Fig. 2.2.2.1 A) and hMSC-tert cells (not shown). As even low-level cellulase expression may lead to degradation of the cellulose sheet over time, it is necessary to use a tightly regulated system in order to avoid premature rupture of the cellulose membrane. It was therefore necessary to reduce leakiness of cellulase expression from pCK71. In order to achieve this, we used a 3'-UTR mRNA destabilizing elements, that have previously been reported to reduce the half-life of mRNA and therefore reduce basal expression levels (45). Two destabilizing RNA ARE elements (AU-rich mRNA destabilizing Elements) (45) were cloned at the 3' termini of the cellulase coding region (plasmid pMFl04). mRNA destabilization has been shown to lead to about 10-fold reduced leakiness, albeit at the expense of approximately 3-fold reduced maximal expression (11; D. Ausländer, unpublished data). Comparison of pCK71 and pMFl04 in HEK 293T and hMSC-tert showed that use of AREs indeed lead to approximately 3-fold reduced maximal expression, but also to 6-10 fold reduced leakiness (Fig. 2.2.2.1 B). In this context, reduced maximal expression is not a considerable drawback, as *in vitro* tests with the cellulose-switch sensor indicated that it can successfully sense cellulase even at these reduced levels. Cellulase expression was also tested in the presence RTP1S. Co-expression of RTP1S with cTAAR1 and cellulase reduced leakiness and increased fold induction both with the previous cellulase expression vector pCK71, as well as destabilized mRNA cellulase expression vector pMFl04 (Fig. 2.2.2.2 A-B).

This was confirmed by *in vitro* experiments performed with culture supernatants of hMSC-tert (induced to express cellulase with Guanabenz) (Fig. 2.2.2.2 C). In this experiment, hMSC-tert were seeded onto cytodex 1 microcarrier beads before induction, to better simulate the conditions they would encounter within the medical implant. Despite the use pMFl04 with cellulase destabilized elements, considerable leakiness was nevertheless present, and caused the sensor to activate after a long incubation period (see Fig. 10). Increased leakiness after seeding cells onto cytodex was likely due to the requirement for trypsinization and re-seeding of cells after transfection (see section **2.3.1** for discussion) and indicates that that RTP1S co-transfection, or stable cell line engineering may be required to reduce leakiness further.

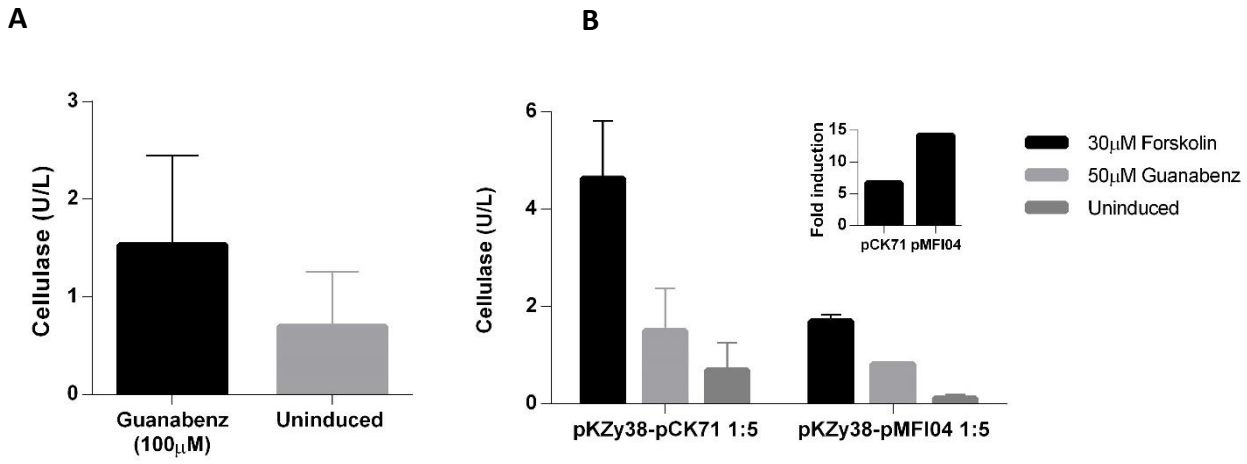

Figure 2.2.2.1 Destabilizing 3' mRNA elements (ARE) reduce leakiness in cellulase expression. (A) HEK 293T transfected with pKZy38-pCK71 (cTAAR1-cellulase). Uninduced cells show considerable background expression of approximately 0.8 U/L. **(B)** HEK 293T cells transfected with pKZy38 (cTAAR1) and either pCK71 or pMFl04 (a plasmid engineered from pCK71, whereby small destabilizing RNA elements – ARE, is added to the 3' of the cellulase mRNA). Compared to pCK71, pMFl04 shows considerably reduced leakiness and increased fold induction (inset) although also reduced maximal expression levels.

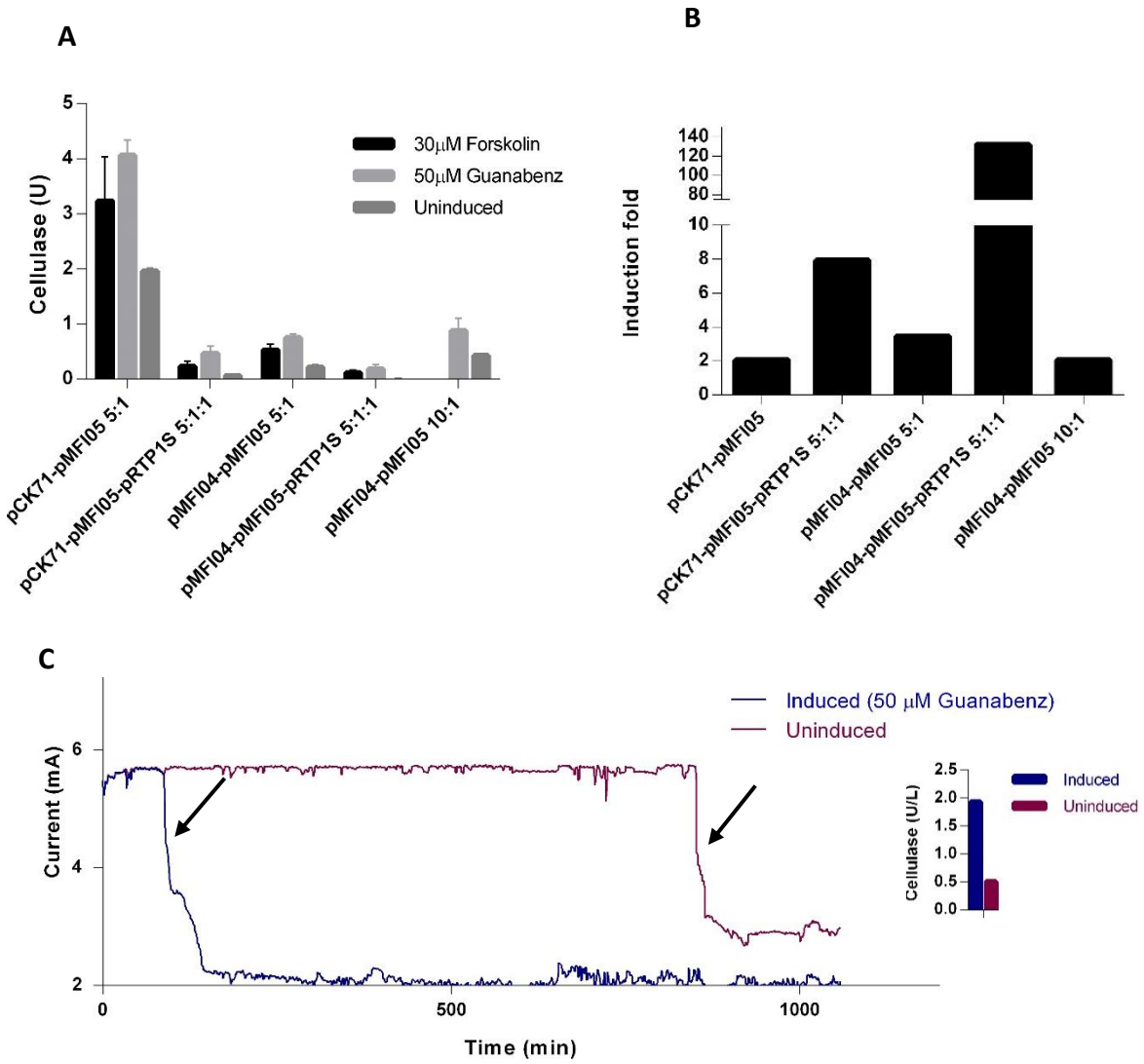

Figure 2.2.2.2 Destabilizing 3' mRNA elements (ARE) and cotransfection of pRTP1S reduces cellulase expression leakiness in hMSC-tert. (A) hMSC-tert transfected with pMFl05 and pCK71, pMFl04 and/or pRTP1S at different ratios. **(B)** Fold induction between induced and uninduced cells for each treatment. Both usage of pMFl04 and cotransfection of pRTP1S reduce leakiness, and lead to increased fold induction. Cotransfection with both pMFl04 and pRTP1S leads to close to undetectable leakiness, and as a result a very high fold induction, however also reduces cellulase maximal expression over 10-fold. Therefore, depending on the ultimate requirement of the implant, it may be worthwhile to use either pMFl04, pCK71 with pRTP1S or pMFl04 with pRTP1S. **(C)** hMSC-tert transfected with pMFl05-pCK71-pRTP1S at 5:1:1 ratios, reseeded onto cytodex 1, induced with 50 μM Guanabenz and cellulose sensor placed into the supernatant 48h later. Measurement of cellulase concentration at that time showed considerable leakiness (inset), as had been observed with other experiments using cytodex (see section 2.3.1 for discussion). Both induced and uninduced cultures activated the cellulose sensor (arrows).

2.2.3 Modular GPCR-based cellulase expression

In order to extend this proof of concept of a synthetic transduction system to other GPCR biosensor modules; cellulase expression was tested in response to a set of different GPCRs. These included the olfactory receptor OR7D4 bonobo, and its cognate ligand androstadienone, OR51E2 (propionic acid), GBPA (deoxycholic acid), OREG (eugenol), and MOR9-1 (vanillic acid). Although expression levels and fold induction varied between different GPCRs, and were generally lower than for the optimized cTAAR1-cellulase circuit, all GPCRs showed induction of cellulase expression in response to their ligands without initial optimization (Fig. 2.2.3). This indicates that different GPCRs can signal through the same PKA pathway to activate cellulase expression, and that this system is therefore modular and broadly applicable to sense any biochemical signals sensed by a GPCR.

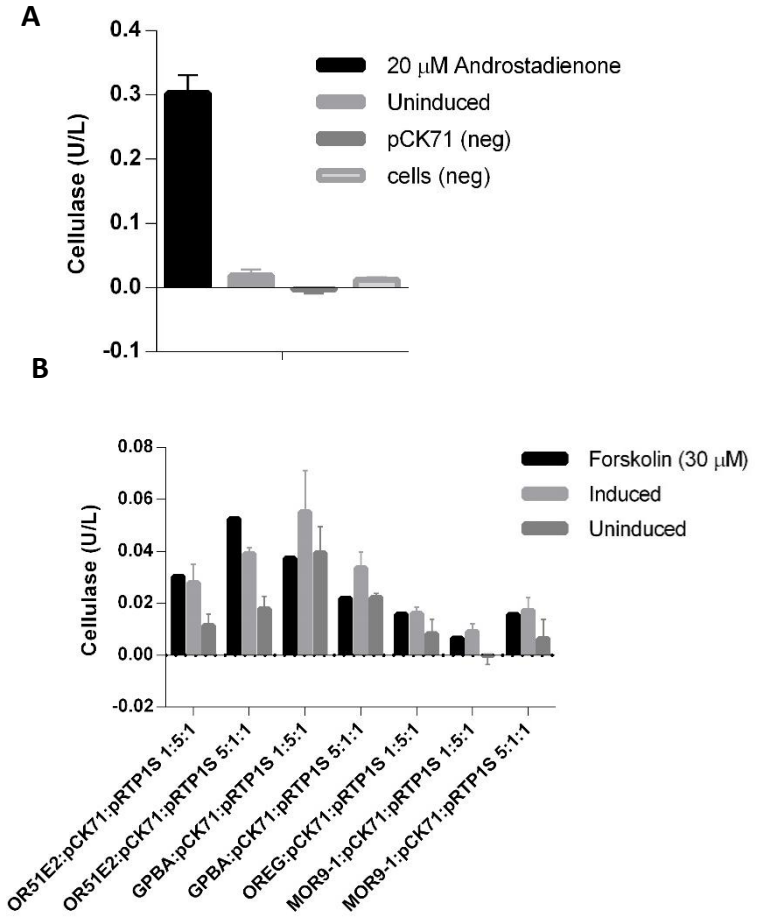

Figure 2.2.3 Cellulase can be modularly induced by a range of GPCRs. (A) HEK 293T transfected with pOR7D4bonobo and pCK71 at 1:5 pOR7D4:pCK71 ratios, induced with 20 μM Androstadienone, and cellulase quantified 48h post-induction. **(B)** HEK 293T transfected with a range of GPCRs at various ratios, induced with their cognate ligands, and cellulase quantified 48h post-induction. Forskolin was used as positive control of induction. GPCRs were induced as folllowing: OR51E2 with 3 mM propionic acid (adjusted to pH 7), GPBA with 100 μM deoxycholic acid (DCA), OREG with 100 μM eugenol and MOR9-1 with 200 μM vanllic acid.

2.3 Minimization of NIR light-based control system

Previously, a wirelessly powered NIR light system was engineered to control gene expression of transgenic cells within an implant. (16). In this system, a 5 mm diameter LED was used with a three-dimensional power receiver antennae to control transgene expression of HEK Freestyle cells engineered with the DGCL pathway (16). However, in order to use a NIR based (or other light-based) gene expression control within the context of an RFID-powered medical implant, several improvements to the system were required. Firstly, it was necessary to use smaller LEDs that could fit into a thin implant, yet be powered with a 2D RFID compatible antenna. Furthermore, it was necessary to maintain the cells in a thin-sheet cell chamber on tissue scaffold and optimize the light system for induction of cells within such a thin-sheet chamber. Finally, it was necessary to optimize the system for use with the medically relevant hMSC-tert.

2.3.1. Using cytodex 1 as a cell scaffold

For a scaffolding agent, cytodex 1 microcarrier beads were chosen as the scaffold of choice. Cytodex 1 beads are low-cost, commercially available small 150-250 μm diameter beads, composed of cross-linked dextran matrix that is substituted with positively charged N, N-diethylaminoethyl groups throughout the matrix. Although cytodex 1 microcarriers are non-degrading, and thus take up space within the implant, they may potentially be used to streamline cell culturing and loading into the implant, by allowing cells to be grown and loaded directly onto cytodex, without the need for prior trypsinization and re-seeding. This may be a considerable advantage, since trypsinization can cause cell stress and apoptosis, which may lead to increased immunogenicity within an implant. The loss of space (compared to using biodegradable scaffolds) however may be made up by the use of a slightly (300-500 μm) thicker cell chamber, which does not considerably add to the overall thickness of the implant. While the improved thickness of the cell chamber may reduce oxygen diffusion compared to a very thin (100-200 μm) cell chamber, it is expected not to result in considerable reduction of oxygen availability, as cells growing on non-degradable scaffold would also be present at lower overall densities within the implant (compared to cells growing into a continuous tissue sheet in biodegradable scaffolds (14)), thus leading to overall lower oxygen requirement per unit volume.

Testing of hMSC-tert and HEK293T with cytodex 1 showed that they can easily attach to and grow on the substrate beads (Fig. 2.3.1 A), and be induced for transgenic gene expression (not shown). However, preliminary tests also indicated that PEI-mediated transfection is inhibited by the presence of cytodex, resulting in 3-6 fold decreased efficiencies (Fig. 2.3.1 B), and that trypsinization and re-seeding of cells onto cytodex after transfection results in lower fold induction (not shown). The reason for this is unknown, but likely occurs due to re-seeding after transfection, which may lead to both reduced maximal expression due to plasmid loss, and increased basal expression due to cell stress, together leading to a reduced induction range. It is therefore likely that stable cell lines or transiently transfected cell lines that have not been re-seeded after transfection will show a higher fold induction using the same genetic circuits.

2.3.2 Testing and minimization of the NIR system

In order to meet the requirements of a smaller LED and a medically relevant cell chamber, 3D printing was used to rapidly prototype different designs for cell chambers by the author, and different LEDs were tested with different induction conditions.

To minimize the NIR LED to relevant dimensions, three NIR LEDs (5mm, 3mm and 1.2mm in diameter) were tested for their ability to induce gene expression in HEK 293T and hMSC-tert transfected with pKZy113/pSO4 (encoding P_{SV40}-DGCL-pA and P_{CMV}-DGCL-pA respectively), pSTING (P_{CMV}-STING-pA) and pSO3 ($P_{INF\text{-}ACD)}$-SEAP-pA). Tests were carried out either on culture plates or within implants (Fig. 2.3.2.1 A). Tests of transfected HEK 293T cells seeded on tissue culture plates using maximal current (50mA) indicated that the smallest LED was equivalent to the two larger LEDs (Fig. 2.3.2.1 B). Similarly, small LED was able to effectively induce hMSC-tert transfected with the NIR inducible DGCL pathway (Fig. 2.3.2.1 C). Similarly, in tests of transgenic HEK 293T seeded on cytodex and induced within the implant, the smallest LED performed comparably to the largest 5mm LED (not shown). In order to test whether maximal induction could also be achieved with lower current, at the order achievable by the RFID chip (around 10 mA), transfected HEK 293T cells were illuminated at different currents for different periods of time. Although decreasing current showed a clear decrease in induction efficiency, maximal induction could nevertheless be achieved by increasing the illumination time (Fig. 2.3.2.1 D), indicating that the small LED, used at RFID-relevant currents can be used to induce cells within the implant. As the use of the small LEDs allowed for a considerable reduction in implant thickness, and was therefore used in all further developments.

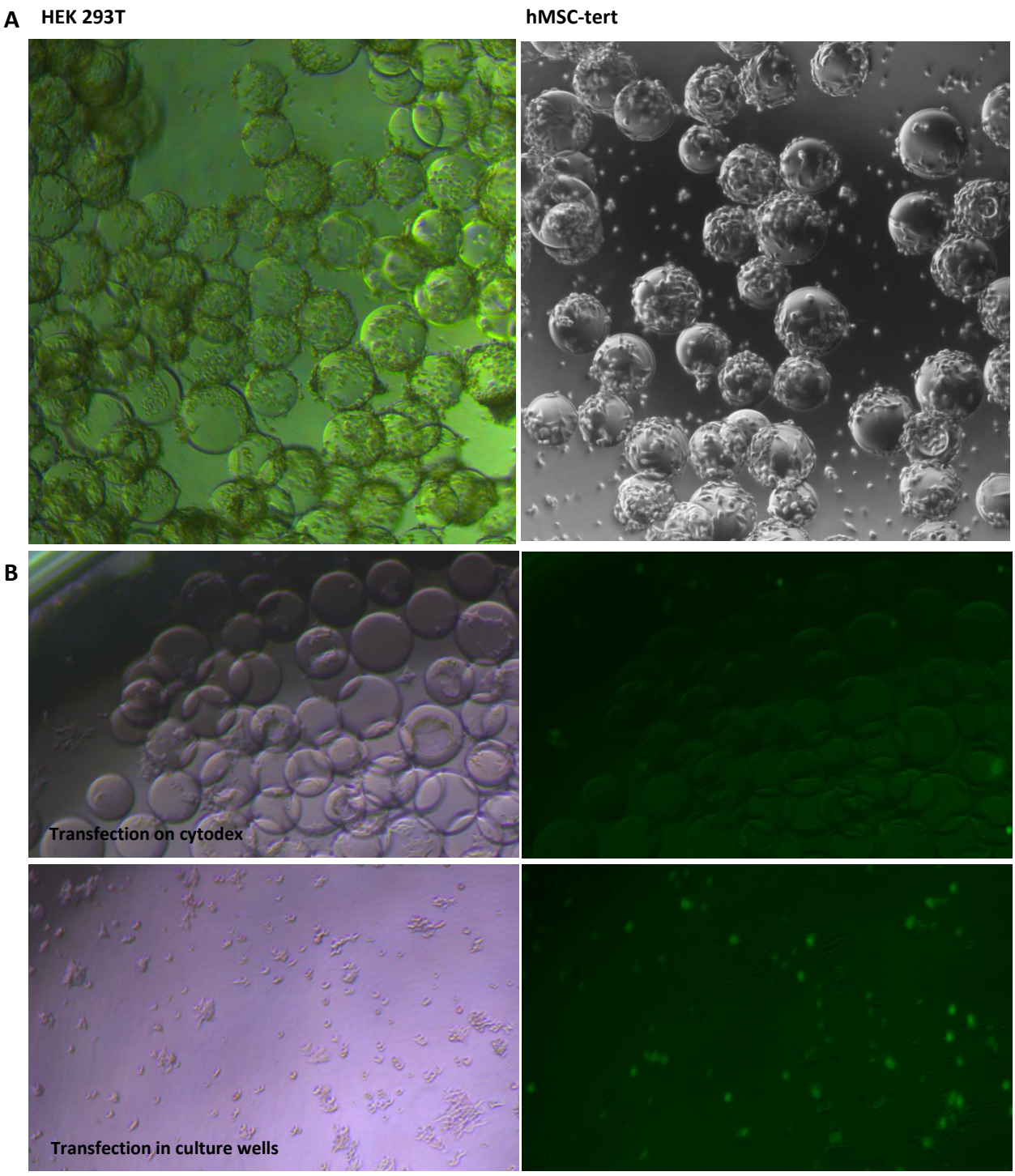

Figure 2.3.1 Use of cytodex 1 for cell culturing. (A) Morphology of HEK 293T (left) and hMSC-tert (right) after 2 day growth n cytodex. Both HEK 293T and hMSC-tert can readily attach to and grow on cytodex. **(B)** Equal numbers of HEK 293T transfected with GFP either when growing on cytodex or within culture dish. Transfection of cells on cytodex results in considerably lower transfection efficiencies, as estimated from the number of GFP positive cells (right).

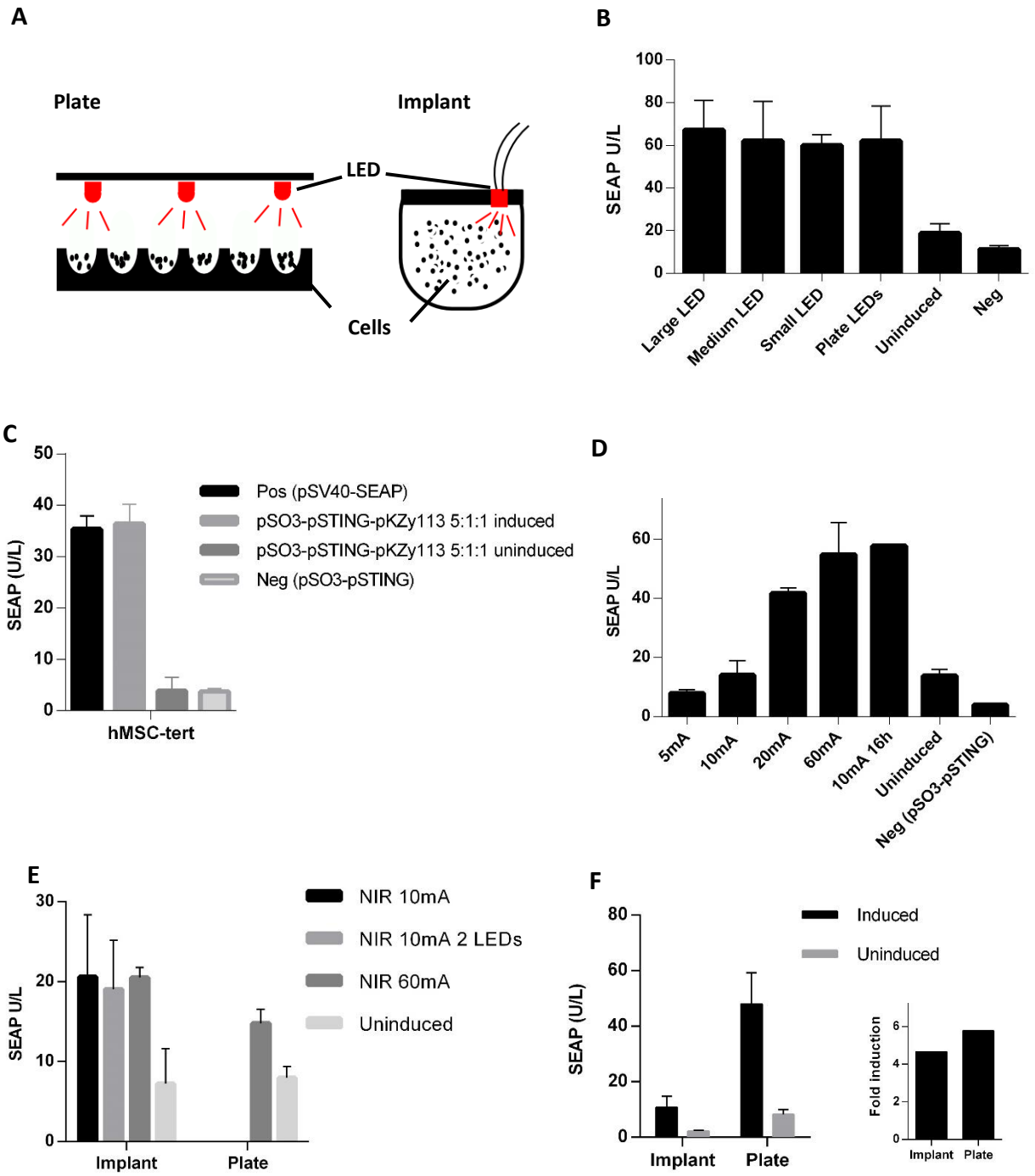

Figure 2.3.2.1 Minimization of NIR LEDs and usage in hMSC-tert. (A) Comparison of NIR induction on cell culture plates vs inside an implant. In cell culture plates, LEDs are placed above the cells (covered with a transparent plastic lid), while inside implant, is placed into the wall of the implant. In implant, cells are always seeded on cytodex, while on plates, can either be attached to the plate, or seeded onto cytodex. **(B-C)** HEK 293T transfected with 5:1:1 pSO3 (pINF$_{\beta(ACD)}$-SEAP-pA), pSTING (pCMV-STING-pA) and pKZy113 (pSV40-DGCL-pA) attached on plates. pKZy113 was used instead of pSO4 (pCMV-DGCL-pA), since the latter showed very high leakiness inboth hMSC-tert and HEK 293T, whereas pKZy113 behaved optimally in all tests. Transfected cells were illuminated with NIR using different size LEDs (5mm, 3mm and 1.2mm diameter), and a positive control plate LED at 60 mA, 3h.As all LEDs resulted in similar induction, the smallest LED was used in further experiments. **(D)** HEK293T transfected with 5:1:1 pSO3, pSTING and pKZy113 and induced with the small LED at different currents for 3 hours. At 10mA, which is the current achievable in the RFID chip, expression level is reduced compared to 60 mA full illumination. This however can be made up by longer illumination times, as 16h illumination results in full induction. **(E)** HEK 293T transfected with 5:1:1 pSO3, pSTING and pKZy113, seeded on cytodex, placed either inside implants or on plates, and illuminated with one or two small LEDs for 16 hours. Usage of 60mA current or 2 LEDs do not result in overall greater induction, compared to a single LED powered with 10mA current. The implant geometry and encasing does not preclude light from reaching the cells, as cells induced on plates show similar fold induction. **(F)** hMSC-tert transfectedwith 5:1:1 pSO3, pSTING and pKy113, seeded on cytodex, placed inside implants or on plates, and induced with small LED for 16h at 10mA. hMSC-tert shows induction similarly to HEK293T.

For the engineering of the cell chamber, PLA, ABS and PA 2200 were used as 3D printing materials, as all have been shown to be non-toxic and biocompatible. Although the effects of cell chamber dimensions on cell viability and induction were not systematically tested, *in vitro* induction tests with cells loaded in the implant showed a similar level of induction compared to cells induced in cell culture plates, indicating that cell chamber dimensions were not limiting NIR light exposure to cells (Fig. 2.3.2.1 E-F). Note that higher total SEAP levels on plates were likely caused by a 3x lower volume of media on plates, whereas fold induction remained the same for both (Fig. 2.3.2.1 F). Furthermore, tests with different light guides showed no improvement in induction, supporting this conclusion (not shown), in total indicating that the miniature NIR light system can be used within the flat-sheet implant to successfully induce gene expression.

With regards to light guides, it must also be noted that the experiments were preliminary and may have a different result (e.g. faster induction) when more advanced light guides are used, as visually it is clear that the red light concentrates near the LED in the current system.

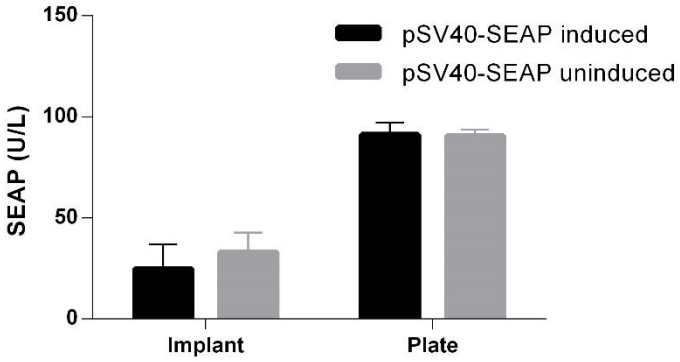

Figure 2.3.2.2 Testing for adverse effects of continuous NIR illumination. HEK 293T cells transfected with pSEAP2-Control (pSV40-SEAP-pA), seeded on cytodex, placed inside implants or on a culture plate and illuminated with NIR light for 16 hours to test for heating, or any other potential cytotoxicity of long-term NIR illumination.

2.4 Stable cell line engineering

2.4.1 Overview of stable cell line engineering strategy

In order translate the therapeutic circuits into medical applications, it is necessary to engineer stable cell lines expressing the GPCR-cellulase sensor circuit, and the NIR light inducible therapeutic circuit respectively. To allow modularity and compatibility with the implant, a strategy was undertaken whereby the GPCR-cellulase circuit is stably integrated into one, "sentinel" cell line, and the NIR inducible therapeutic circuit integrated into a second "therapeutic" cell line. This approach has several advantages over integrating both circuits into the same cell line, as:

a) It allows therapeutic and sentinel cell lines to be used alone when necessary.
b) It allows the therapeutic and sentinel cell lines to be combined with different ratios, instead of a single fixed ratio.

c) It simplifies the stable cell line production process, as making of two cell lines requires genome integration of three components each, instead of six components required for making a single cell line containing both circuits.
d) It simplifies the exchange of GPCRs in the sentinel cell line, and therapeutic output proteins in the therapeutic cell line.

As previously stated, for development purposes, a Guanabenz-inducible GPCR cTAAR1 was chosen as the GPCR for the sentinel cell line, and SEAP chosen as the output for the NIR controlled therapeutic cell line. These are the circuits, with which the first stable cell lines are engineered. To create the stable cell lines, a cloning strategy was devised, whereby the components of the sentinel and therapeutic circuits would be cloned into lentiviral vectors, and stable cell lines generated by co-transduction of the components of both circuits into separate hMSC-tert cell lines, followed by induction and positive/negative screening of cells with FACS. In order to allow FACS screening of successfully transduced cells, YFP and RFP would be fused via IRES linkers to the cellulase gene in the sentinel cell line and to SEAP in the therapeutic cell line respectively, and cells FACS screened for high fluorescent reporter expression after induction, and for low fluorescent reporter expression after removal of inducer. This strategy selects for a population in which cellulase and SEAP respectively are specifically expressed only in response to induction.

While the Guanabenz-inducible cTAAR1 and SEAP are useful for development purposes, it is necessary to allow modular exchange of cTAAR1 in the sentinel cell line, and of SEAP in the therapeutic cell, in order to allow these lines to be used for further therapeutic purposes. To allow this, cTAAR1 expression construct in the sentinel cell line, and SEAP expression construct in the therapeutic cell line were flanked by FRT (Flp-recombinase target) sites, which are recognized by the FLP (flippase) site-specific recombinases. FLP-FRT recombinase was chosen over cre-lox recombinase, because FLP recombination efficiencies are comparable or higher than the cre-lox recombination efficiencies, but the latter is known to be highly active, capable of catalysing recombination between distant sites if more than one pair of homologous FRT are integrated into the genome (46). Flanking of these genes with FRT sites allows them to be replaced by other genes via recombinase mediated cassette exchange (RMCE). Therefore, once functional "master" sentinel and therapeutic cell lines with cTAAR1, and SEAP respectively have been established, it should be possible to modularly exchange cTAAR1 and SEAP for other genes, without the need to generate new stable cell lines for scratch (see Fig 2.4.1 for construct designs). .

2.4.2. Lentivirus cloning

To realize this strategy, a 3rd generation lentiviral vector lentiCRISPRv2 (47) was chosen as the integration vector. This vector was chosen specifically, as it has undergone extensive testing and development, and has been optimized for high gene expression and lentiviral titer production (47). In order to create the cell lines it was necessary to clone the 6 required components (P_{SV40}-SEAP, P_{CMV}-STING and $P_{INF\text{-}\beta(ACD)}$-SEAP for therapeutic cell line, and cTAAR1, P_{CRE}-cellulase and possibly P_{CMV}-RTP1S for the sentinel cell line), into the lentiCRISPRv2 backbone. To clone the components, it was first necessary to exchange the gRNA-Cas9 genes in lentiCRISPRv2 for a multiple cloning site, which could then be used as basis to clone in the rest of the components. During attempts to do this, it was necessary to re-design cloning methods several times, due to the difficulties associated with amplifying segments of the vector with PCR. However, using classic restriction-enzyme mediated cloning, these efforts ultimately yielded a backbone with gRNA-Cas9 substituted for a multiple cloning site (plasmid pMFl08) containing 5' KpnI, NheI, XhoI, XbaI, FseI, EcoRV, BamHI 3' sites (see Fig. 2.4.2 for plasmid map). Although it was not possible to finish cloning of the rest of the components due to time constraints, this backbone allows other components to be cloned using straightforward restriction-enzyme mediated cloning, and therefore represents a good resource for cloning of lentiviral integration vectors in general.

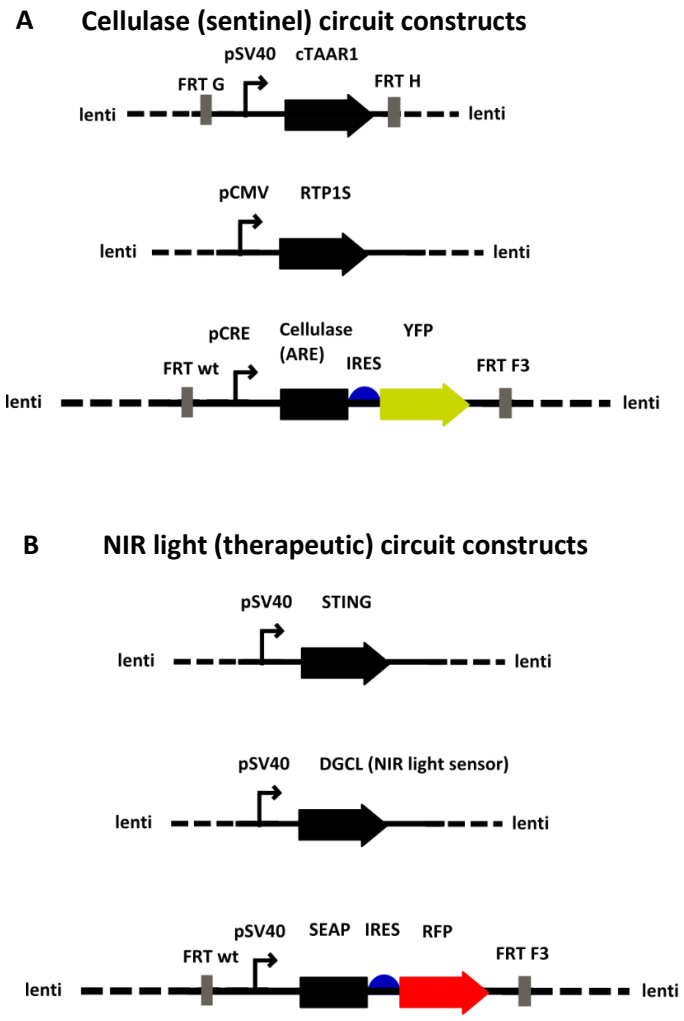

Figure 2.4.1 Lentiviral constructs for engineering stable sentinel and therapeutic cell lines. (A) Cellulase circuit constructs for engineering stable sentinel cell lines. Cellulase is linked to YFP expression through an internal ribosomal entry site (IRES), in order to detect successful cellulase expression during screening. Both cellulase and cTAAR1 expression cassettes are flanked by orthologous FRT sites, which enable FLP-mediated recombineering after integration into the genome. **(B)** NIR light circuit lentiviral constructs for engineering stable therapeutic cell lines. Here, SEAP expression is linked to RFP expression via an IRES sequence, and the expression cassette is flanked by orthologous FRT sites to enable FLP-mediated recombineering.

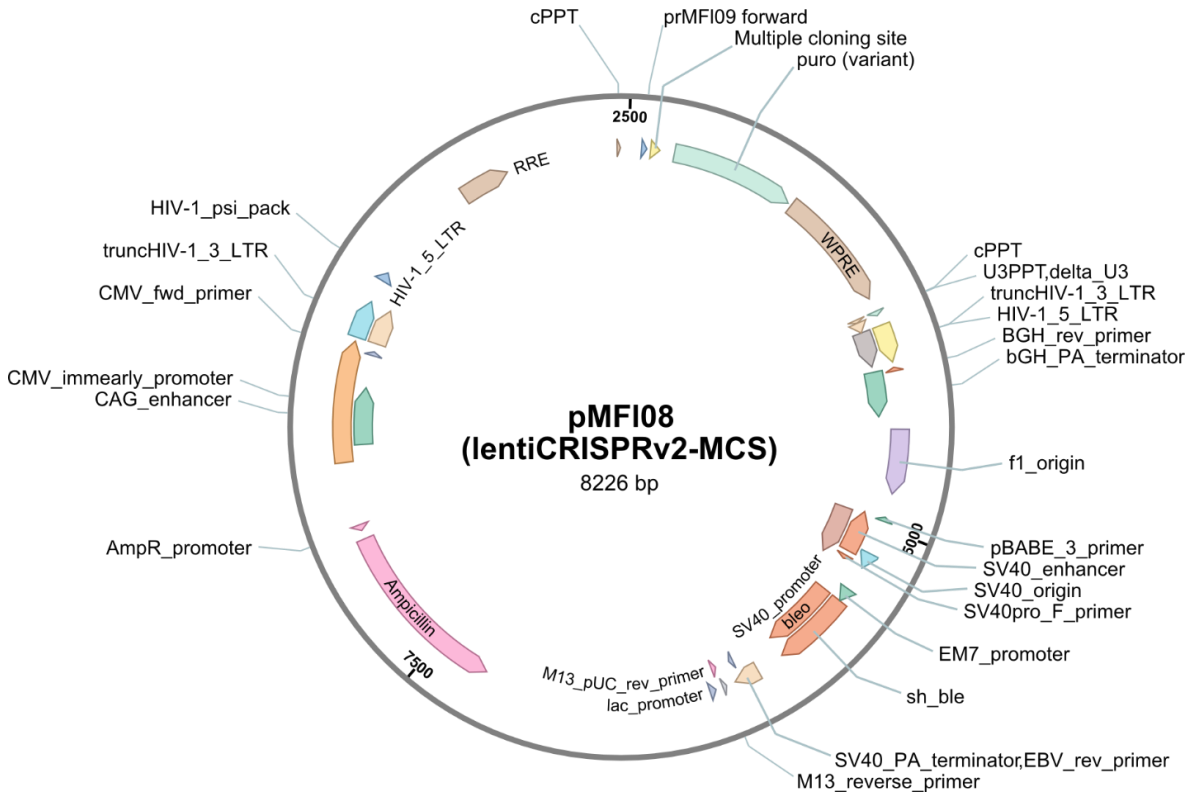

Figure 2.4.2 pMFL08 plasmid map. Multiple cloning site was cloned 5' of the puro (variant) sequence, and 3' of the cPPT.

2.5 RFID chip and implant engineering

To allow for wireless power and signal transmission, and integration of all components, a custom-made RFID and implant encasing were engineered.

2.5.1 RFID engineering

The RFID dimensions were designed based on constraints imposed by the maximal size of the implant, required size of the cell chamber, and required power by the LED light. To match these demands, a design whereby the RFID chip's antennae runs alongside the outer border of the implant was created by the author, and the RFID chip's circuitry and componentry designed, assembled and tested by Peter Buchmann, ETHZ (Fig. 2.5.1.1). The RFID is powered by a transponder coil, emitting 13.56 MHz radio waves (designed by Peter Buchmann, ETHZ). The RFID chip consists of a 0.4mm PCB board with wet-etched copper interconnects, and various componentry soldered onto both sides to convert the alternative current collected by the RFID receiver antennae to direct current (required by the LED and cellulase sensor), and power a frequency divider chip that modulates the receiving 13.56 MHz input radiofrequency into 12.9 and 14.4 MHz output radio frequency, which can be used to wirelessly transmit data from the cellulase sensor (Fig 2.5.1.2).

This design allowed a maximal current of 10 mA within the LED, necessitating longer induction times to achieve full induction (8-16 hours) (Fig. 2.3.2.1). Despite longer induction times, induction of both transgenic HEK293T and hMSC-tert could be achieved by the wirelessly-powered RFID, with no observed heating or other adverse effects on the cells, indicating that the RFID and the LED powered long-term with a 10 mA voltage is suitable for induction in a medical setting (Fig . 2.3.2.2).

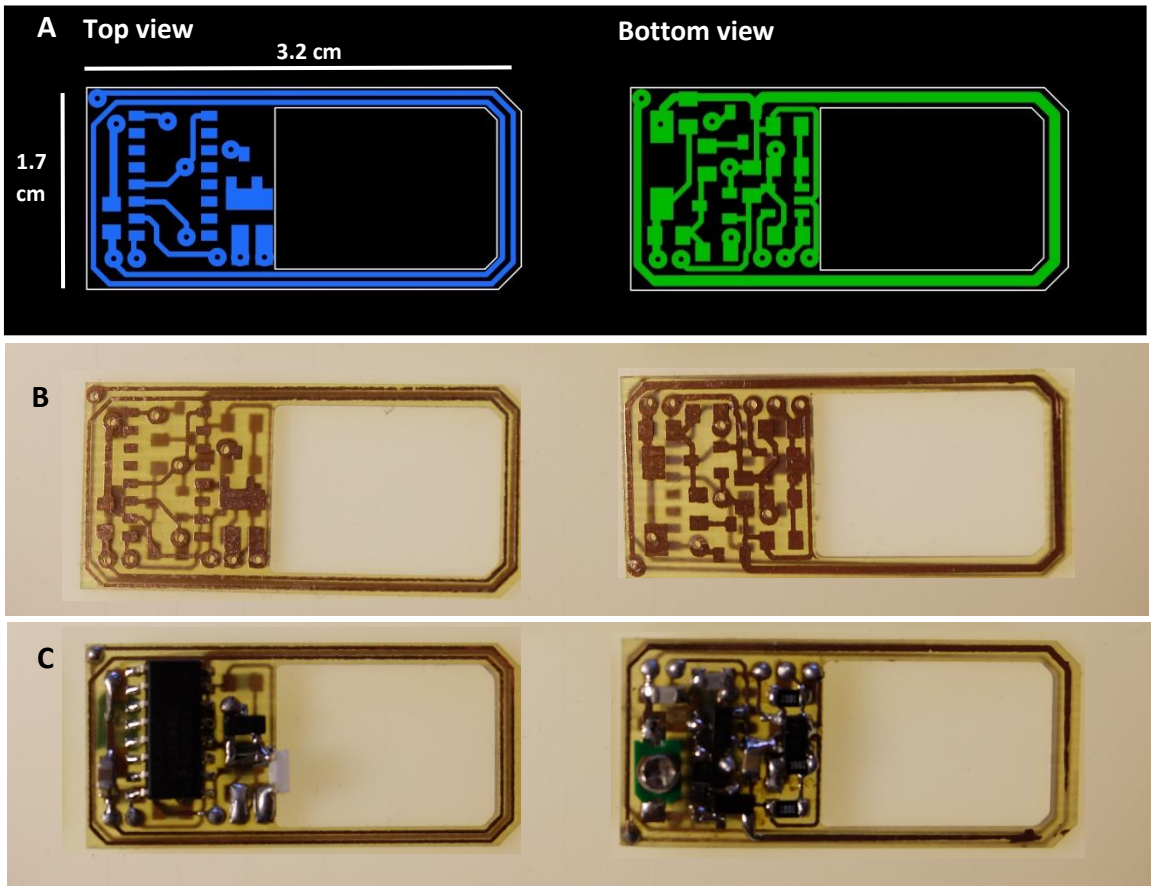

Figure 2.5.1.1 RFID chip design and engineering. (A) Designed copper traces for top and bottom layers. **(B)** Bare PCB board with copper layers. The outermost copper layers circling the board act as energy receiving antenna, while the central layers act as interconnects for RFID componentry **(C)** Complete RFID chip with soldered RFID componentry. RFID chip and field generator designed and built by P. Buchmann (ETHZ) in collaboration with the author.

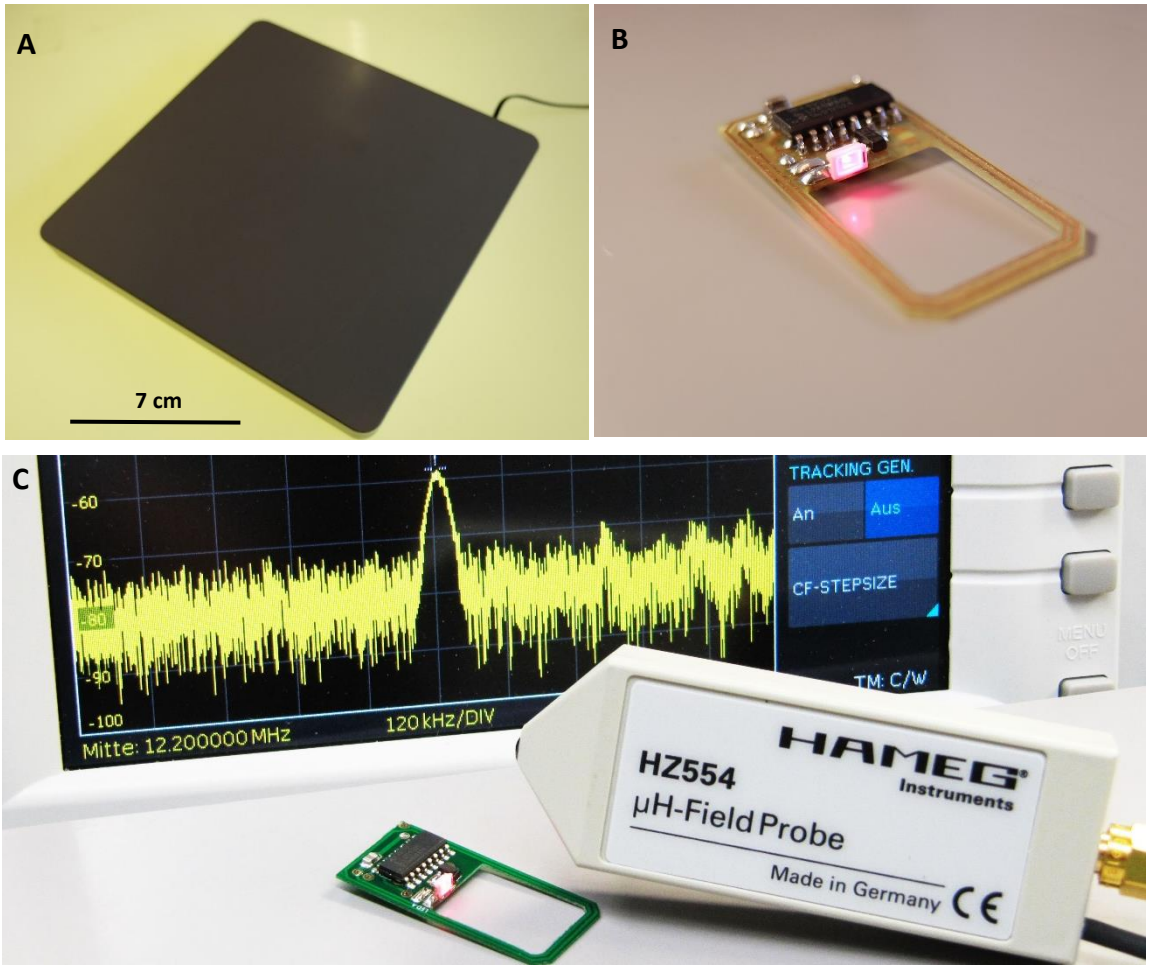

Figure 2.5.2.2 RFID chip functioning. (A) Field generator plate. **(B)** RFID chip powered on active field generator to emit NIR light. **(C) RFID** signal transmission – detected as an active peak at 12.2 MHz (top) by a a radio frequency analyser receiving antenna (right to the chip). RFID chip and field generator designed and built by P. Buchmann (ETHZ) in collaboration with the author.

2.5.2 Implant encasing

For prototyping the design of the implant encasing, PLA and ABS were initially used by the author to determine critical implant dimensions. However, PLA and ABS cannot be 3D printed well at sub-millimetre accuracy, as the printing process requires additive extrusion of each layer to achieve the final print. In order to solve this problem, laser light-based printing using Formlabs Standard resin and PA 2200 was tested. Although both could achieve detailed sub-millimetre accuracy, Formlabs standard resin proved highly cytotoxic, even when covered by an insulating layer of Epotek 301 medical glue, or polyurethane-based insulation. PA 2200 was therefore used for all further tests, prints ordered by a commercial vendor, and design continuously improved over design-build-test cycles. As a final design, an implant with the wall thickness of 0.3 – 0.4 mm and a total size of 33.8 x 16.6 x 5mm was created (Fig 2.5.2.1). This size is the result of several cycles of optimization, and represents the most possible compact implant achievable by the constraints of the RFID chip and cell chamber sizes. The completely assembled implant was capable of collecting power as efficiently as a stand-alone RFID chip based on visual inspection, indicating that the addition of an LED, microswitch and implant encasings did not interfere with power collection (Fig. 2.5.2.2). Furthermore, both the microswitch and the LED functioned similarly in the assembled implant, as they did stand-alone. This implant is therefore a functional prototype of a device capable of wirelessly sensing and treating disease.

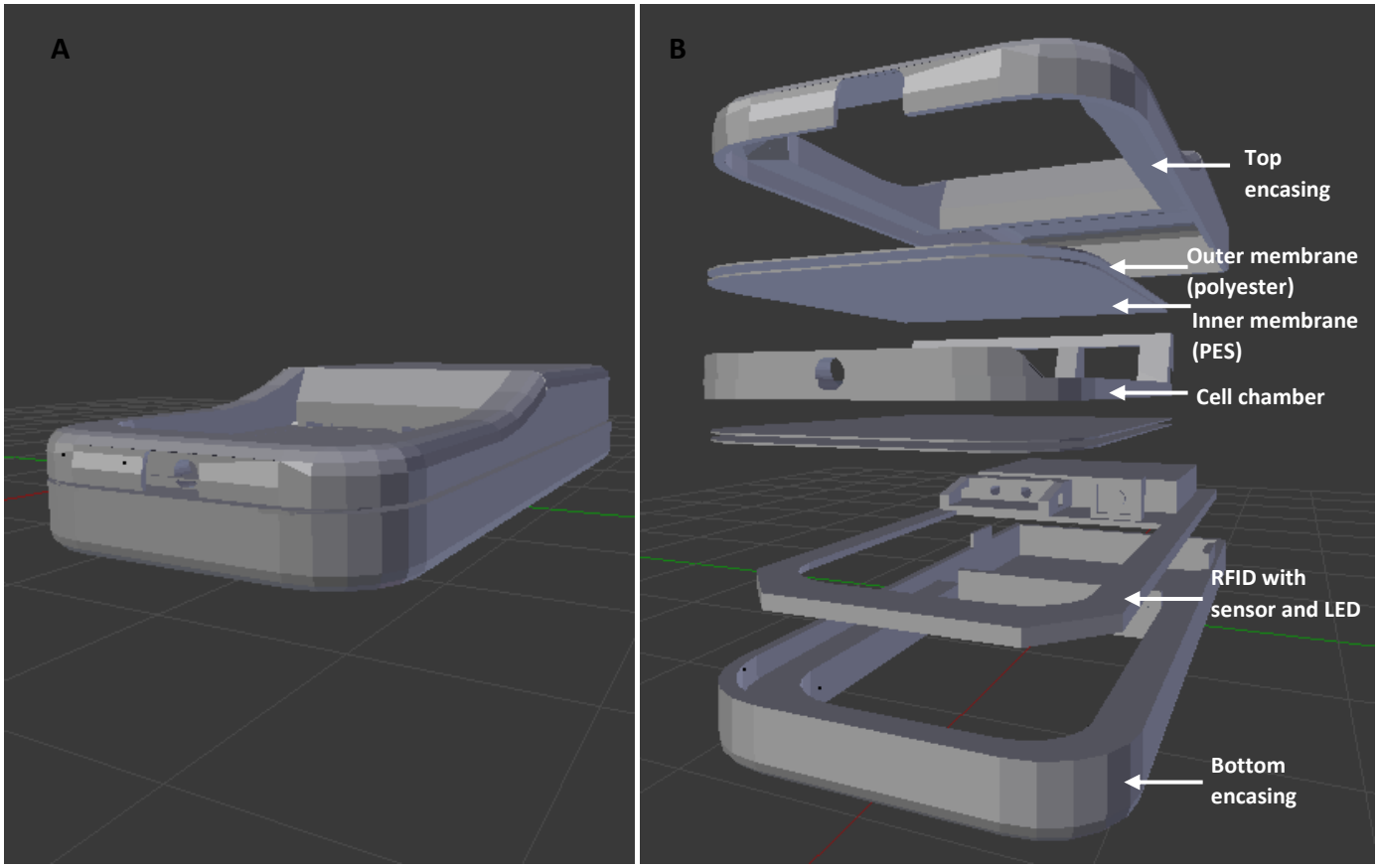

Figure 2.5.2.1 3D design of the implant. (A) Implant overview **and (B)** implant components in exploded view, with components pointed out using arrows.

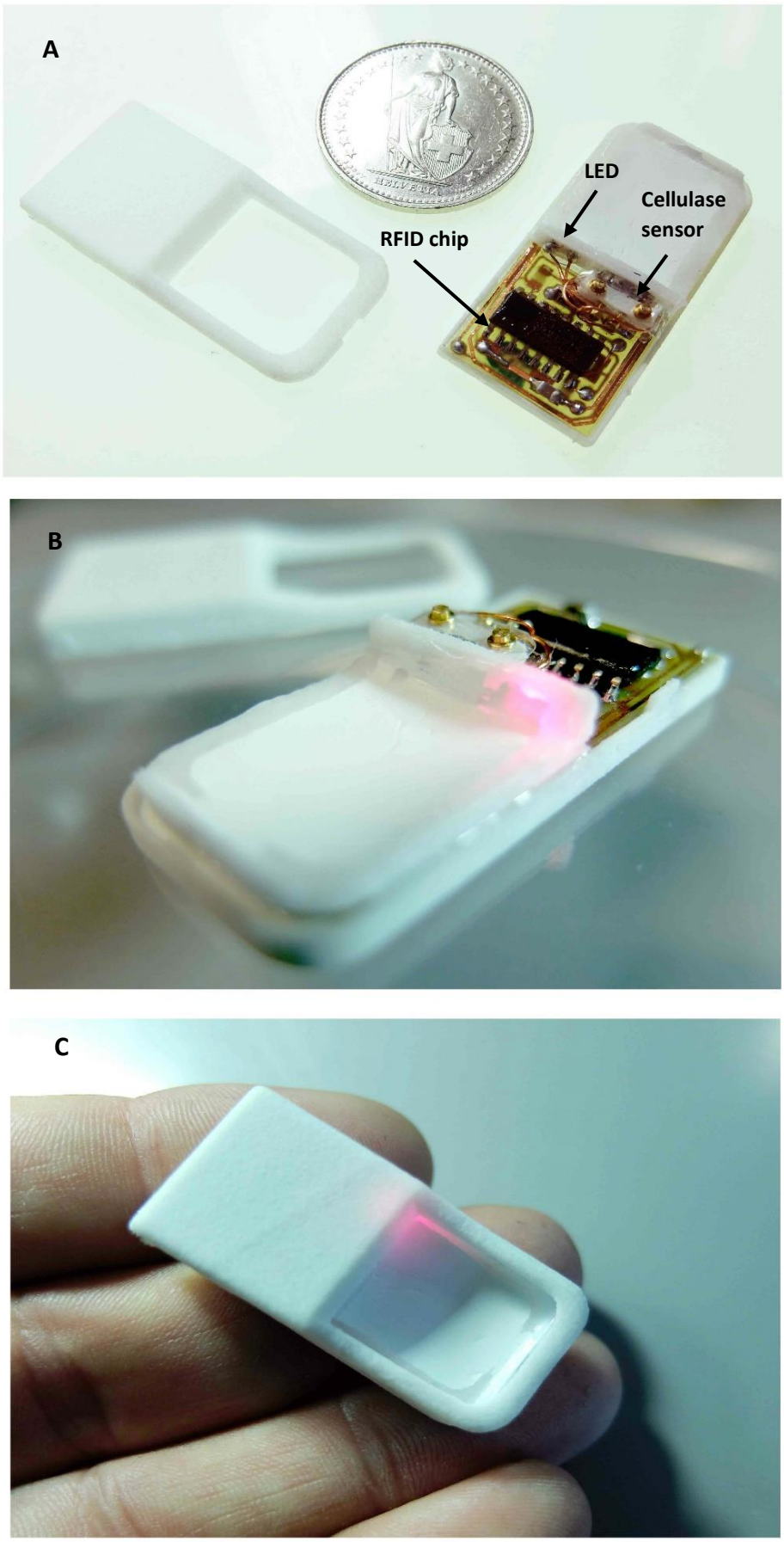

Figure 2.5.2.2 Assembled implant. (A-B) Front and back view of PA 2200 3D printed implant encasings and cell compartment, with RFID chip, LED and cellulase sensor inserted (marked with arrows). **(C) I**mplant activated on field generator to emit NIR ligth, held approximately 2 cm from the surface of the generator plate.

III Conclusions and Outlook

The goal of this project was to engineer a next generation medical implant that can sense and wirelessly transmit information about disease biomarkers or other molecules of interest, and in conjunction use light to control production of therapeutic proteins. For this end, two cell lines were designed. The first, "sentinel" cells were engineered to sense disease biomarkers through GPCRs, and signal this input to the implant by producing cellulase, that is then sensed by a miniature cellulase sensor within the implant. The GPCR chosen for development purposes here was cTAAR1, inducible by the xenogeneic molecule Guanabenz. The second, "therapeutic" cell line, houses a near infrared-light inducible diguanylate cyclase, which controls the production of therapeutic protein(s), and can be induced by near infrared light emitted by the implant. The output protein chosen for testing purposes was SEAP, as it can easily be quantified in the circulation. To integrate these capabilities, a new cellulase sensor was designed to convert the cellulase output of sentinel cells into an electric signal, a new RFID-based chip was designed to collect power and transmit data wirelessly, and a new implant and cell chamber were designed to allow long-term cell growth and vascularization and nontoxic and biocompatible implantation into patients. This system has a large range of applications, and can potentially be used for multiple purposes. However, before it can be applied, some work still remains with respect to finishing and testing the system.

3.1 Outstanding work

Firstly in the area of cell lines, although both sentinel and therapeutic circuits functioned when delivered as transiently transfected plasmids, for mouse studies and medical applications it is necessary to create stable cell lines, where these circuits are stably integrated into the genome, and can function in the long term (months to years). For engineering these cell lines, it is necessary to use medically relevant cell lines hMSC-tert, ARPE19 or others. It is therefore necessary to firstly finish cloning of lentiviral integration vectors, and transduce and screen hMSC-tert and/or ARPE19 with the components of both circuits, to establish stable sentinel and therapeutic cell lines. Secondly, the functioning of these cell lines will also have to be tested in the context of the implant. Finally, although these cell lines can be used to develop the system, and test the implant in first mouse studies, for therapeutic applications, it is ultimately necessary to use recombinase mediated cassette exchange, to swap cTAAR1 and SEAP in sentinel and therapeutic cell lines for therapeutically relevant GPCRs and output proteins respectively.

Secondly, when the sentinel and therapeutic cell lines are established, it is necessary to test the complete system in mouse studies. Currently, mouse studies are planned to take place in Basel or Lyon at the end of 2016 or beginning 2017, whereby 6 cohorts of mice would be used to test both the sentinel and therapeutic output capabilities of the implant. For the therapeutic output, three cohorts are planned be tested – firstly a cohort with the implant, and cells induced by red light, secondly a cohort with the implant, and cells not induced, and thirdly a cohort with the implant and cells induced by red light, but with the cells containing a mock therapeutic circuit. For the sensor capabilities, two cohorts would be tested: one with implant containing sentinel cells, induced with Guanabenz, and one cohort with the implant containing sentinel cells that have not been induced (mouse studies strategy designed by Marc Folcher, ETHZ in collaboration with the author). Finally, one cohort would contain an implant, without sentinel or therapeutic cells, and would be used as a common control for both sentinel and therapeutic aspects of the implant. Therefore, the two main lines of outstanding work are the completion of the project are the engineering of stable cell line, and *in vivo* testing of the implant in mice.

3.2 Potential applications of the implant

This implant was engineered with the main purpose of providing a system that can continuously monitor disease biomarker(s), alert the patient to their presence, and provide a controlled therapeutic output. For this purpose, a modular GPCR-based sensor system, and NIR light controlled output system was created. Using these systems, the implant can be used to monitor and/or treat a multitude of chronic disease where protein or small-molecule blood biomarkers as well as protein-based therapeutics have clinically been established (Fig. 3.2). They include:

1. viral chronic disease, such as hepatitis B and C (biomarkers being envelope proteins and other proteins) (48) and HIV (gp120 and others) (49, 50)
2. chronic cancers including colorectal cancer (CEA, CEAR and others) (51), hepatocellular carcinoma (CEA, AFP, bile acids) (52, 53), prostate cancer (PSA, PCA3) (54), gastrointestinal and pancreatic cancer (CA19-9) (55),

3. other conditions, including silent myocardial infarction (troponin) (56) and liver cirrhosis (bile acids) (57, 58).

The implant could be used in two different modes. In the first mode, the presence of biomarker is continuously monitored, but therapeutic proteins are not produced before the biomarker levels are high enough to activate the sensor (for example, for prostate cancer patients, in risk of recurrent cancer). In the second mode, the therapeutic protein may be continuously produced, and the sensor used to monitor the return of the biomarker, to determine whether therapy is successful, and alert the user if the condition worsens and treatment must be changed (for example, for HIV infected individuals).

In addition to monitoring disease biomarkers, the implant has potential for use in a range of other applications. For example, instead of a disease biomarker, it may be worthwhile to monitor the appearance of a toxin, viral or bacterial infection, contaminant, or other exogenous signal. This may be useful, for example, in the context of intensive animal farming, where viral and bacterial infections spread quickly and result in considerable losses every year. In this scenario, it may be worthwhile to monitor viral or bacterial infections in livestock, to either treat or euthanize the infected individuals early on before they become infectious to other animals, in order to stop the spread of the infection at its infancy. Additionally, it may also be useful to implant livestock to directly monitor the presence of contaminants or toxins in the milk or meat of the animal, and alert the farmers when their presence is detected. Finally, instead of monitoring disease biomarkers, the sensory function of the implant may be used to monitor a biomarker that indicates the effectiveness of therapy. Here, the therapeutic proteins would be first produced by the genetically engineered cells in the implant, and the sensor function used to measure a secondary biomarker induced by the therapy itself. In this scenario, the sensor would act as a confirmation of a successful therapy, and the lack of its signalling would indicate that implant, or the treatment itself is not functioning as expected.

3.3 Limitations and real-life implementation

Although the implant has a broad range of potential applications, it also has limitations w.r.t real-life implementation.

Firstly, with the current wireless field generator, the RFID chip must be placed relatively close to the implant, approximately 4 cm away, which necessitates a relatively close placement of the implant to the field generator. This range may be improved by using a more powerful wireless field generator, which may increase the range to larger distances. Nevertheless, the field generator will likely have to be relatively close to the patient, in order for the implant to gather sufficient power.

Secondly, long induction times are necessary. In order to therefore implement it in a real life setting, one of two strategies must be used. Either one could develop a wearable field generator that a wearer can attach as a band. Alternatively, one could wirelessly induce the implant during patient's sleep, by placing the field generator underneath the bed or mattress. In these settings, both the requirements for a close proximity and overnight induction times would not be an issue.

Thirdly, the 2D nature of the power-collecting RFID coil means that maximal amount of power is only collected when the implant is perpendicular to the electromagnetic field direction generated by the field generator. Using a standard 2D field generator, this means that the amount of power collected by the RFID chip varies when the chip is tilted, which is necessary to consider in experimental design of mouse studies. For real-life implementation however, it may be possible to create a field generator that generates a concave-shaped magnetic field around the chip, as a result of which the tilted chip would remain perpendicular to the electromagnetic field, and thus collect power at any angles. Alternatively, it may be possible to use a wearable field generator that remains perpendicular to the implant during usage.

Finally, although the cellulase sensor is useful in the context of several disease, the kill-switch nature of the sensor, which can be used to only determine the onset/appearance of the disease biomarker or molecule of interest limits the usage of the sensor to particular applications. For example, it is not possible to continuously monitor a biomarker level, as the sensor is not responsive after the kill-switch type activation. Nevertheless, the applications that can already be targeted with this design are considerably broad. Furthermore, the implant was designed in a fashion, whereby any type of sensor that can produce an on/off electrical signal could modularly replace the cellulase sensor. It is therefore possible to modularly integrate future sensors into the implant,

without the requirement for considerable redesign. The implant therefore represents an engineerable platform for detecting and treating a broad range of diseases.

IV Materials and Methods

4.1 Materials

4.1.1 Equipment

Device	Manufacturer
Autoclave (Varioklav 65 T)	H+P Labortechnik AG, DE
BioPhotometer	Eppendorf AG, Hamburg, DE
CASY cell counter ®TTC	Innovatis systems AG, Roche diagnostics, CH
Centrifuge 5804 R	Eppendorf AG, Hamburg, DE
Centrifuge 5810	Eppendorf AG, Hamburg, DE
Centrifuge miniSpin plus	Eppendorf AG, Hamburg, DE
Heracell 150i CO2 incubator	Thermo Fisher Scientific, Wohlen, CH
Light Microscope Leica	Leica, Wetzlar, DE
Nanodrop 2000 Spectrophotometer	Thermo Fisher Scientific, Wohlen, CH
PJ3600 DeltaRange balance	Mettler-Toledo, CH
PowerPac basic, 400mA, 75W	Biorad, USA
Vortex genie 2	Scientific Industries, USA
Wallac EnVision 2104 Multilabel Reader	PerkinElmer, Massachusetts, USA
Waterbath B-480	Büchi Switzerland, CH
NI myDAQ	National Instruments, USA
NI USB 6008	National Instruments, USA

Table 1. Laboratory and electronics equipment used in the study

4.1.2 Chemicals and Reagents

Name	Manufacturer	Catalogue number
Chemicals		
Biliverdin hydrochloride	Frontier	B655-9-1
Gene Ruler ladder	Fermentas, St. Leon-Rot, DE	SM1351
PEI MAX	Polysciences Inc., Eppelheim, DE	23966
Penicillin/ Streptomycin	Biowest, Nuaille, FR	L0022
Inducers		
1-Octanol	Sigma Aldrich Chemie GmbH, Buchs, CH	74850
4,16-Androstadien-3-one	Molcan Corporation, CA	
5-Androst-16-en-3-one	Molcan Corporation, CA	
Propionic acid	TCI Deutschland GmbH	P0500
Vanilic acid	Sigma Aldrich Chemie GmbH, Buchs, CH	
Molecular biology reagents		
Q5 DNA polymerase	NEB	M0491
Taq polymerase	NEB	M0273S
GeneRuler Ladder	Thermo Fischer	SM0331

Table 2. Chemicals and reagents

4.1.3 Kits

Name	Manufacturer	Catalogue Number
ECL Prime Western Blotting Detection Kit	GE Healthcare, UK	6762621

Jetstar 2.0	Genomed GmbH, Germany	210050
ZR Plasmid Miniprep Classic	Lucerna Chem AG	D4016

Table 3. Kits

4.1.4 Media and Solutions

Name	Manufacturer/Composition
Cell Culture	
DMEM/F-12, GlutaMAX	DMEM (Invitrogen), 10% (v/v) FBS and 1% (v/v) Pen/Strep
Dulbecco's Modified Eagle Medium (DMEM)	DMEM (Invitrogen), 10% (v/v) FBS and 1% (v/v) Pen/Strep
LB Broth	25g LB powder in 1L ddH_2O
Bacterial glycerol stock	10% vol/vol glycerol in ddH_2O added to bacterial culture to 5% glycerol final concentration
Cell freezing solution	10% DMSO, 90% growth medium with FBS and PenStrep (cell-specific)
Reporter Assays	
pNPP	120mM p-Nitrophenylphosphate in SEAP buffer
SEAP Buffer 2X, pH 9.8	20mM Homoarginine, 1mM $MgCl_2$, 21% (v/v) Dietholamine
Transfection	
PEI	Polyethylenimine 1mg/ml
DMEM	DMEM (Invitrogen) without FBS or PenStrep
Gel Electrophoresis	
Agarose gel 1%	1g Agarose in 100ml TEA, 16µl Red Safe
Loading buffer (10ml)	500µl Tris (50mM, pH 7), 2ml 20% Glycerol, bromophenol blue
TAE 50X	2M Tris Base, 2M acetic acid, 50mM EDTA

Table 4. Media and solutions

4.1.5 Cell lines and Bacterial Strains

Name	Specifications
ARPE19	Human retinal neural cell line, immortalized
C2C12	Mouse myoblast cell line, immortalized
Escherichia coli XlBlue	fhuA2 Δ(argF-lacZ)U169 phoA glnV44 Φ80 Δ(lacZ)M15 gyrA96 recA1 relA1 endA1 thi-1 hsdR17
Escherichia coli Turbo	recA1 endA1 gyrA96 thi-1 hsdR17 supE44 relA1 lac [F′ proAB lacIqZΔM15 Tn10 (Tetr)]
Escherichia coli dam-/dcm-	ara-14 leuB6 fhuA31 lacY1 tsx78 glnV44 galK2 galT22 mcrA dcm-6 hisG4 rfbD1 R(zgb210::Tn10) TetS endA1 rspL136 (StrR) dam13::Tn9 (CamR) xylA-5 mtl-1 thi-1 mcrB1 hsdR2
HEK 293 Freestyle	Human embryonic kidney cells, adapted for suspension culture
HEK293T	Human embryonic kidney cells, transgenic for simian virus 40 (SV40) large T antigen
hMSC-hTERT	

Table 5. Cell lines and bacterial strains

4.1.6 Plasmids

Plasmids	Description	Source

lentiCRISPRv2	3rd generation lentiviral backbone plasmid	N. Sanjana (47)
pCI-MOR9-1	P_{CMV}-MOR9-1-pA MOR9-1 expressing plasmid in pCl backbone	H. Matsunami (59)
pCI-OR51E2	P_{CMV}-OR5E2-pA OR51P2 expressing plasmid in pCI backbone	H. Matsunami (59)
pSL2	P_{CMV}-OR7D4b-pA OR7D4bonobo expressing plasmid in pCl backbone	S. Locher (60)
pCI-RTP1S	P_{CMV}-Rtp1s-pA Rtp1s expressing plasmid in pCI backbone	H. Saito (44)
pCK53	P_{CRE}-SEAP-pA	C. Kemmer (11)
lentiCRISPRv2	3rd generation lentivirus vector for gRNA-cas9 expression	N. Sanjana (47)
pMFl04	P_{CRE}-cellulase-ARE-pA in pCK71 backbone Cellulase with 3' destabilizing RNA elements (ARE) added for reduced leakiness.	This work
pMFl05	P_{SV40}-cTAAR1-pA (pSAM200 backbone)	This work
pMFl06	P_{CMV}-cTAAR1-pA (pMM27 backbone)	This work
pMFl07	P_{EF1A}-cTAAR1-pA (pMM28 backbone)	This work
pMFl08	lentiCRISPRv2 with gRNA-cas9 replaced by a multiple cloning site	This work
pCK71	P_{CRE}-cellulase-pA	C. Kemmer (11)
pKZY38	cTAAR1 in pUC57 backbone	K. Zwicky (30, 61)
pWW85	P_{ETR}ON8-CFP-IRESI-RFP-IRESII-YFP-pA	W. Weber (62)
pSAM200	P_{SV40}-SEAP-pA	M. Müller
pMM27	P_{CMV}-SEAP-pA	M. Müller
pMM28	P_{EF1A}-SEAP-pA	M. Müller
pSEAP2-Control	P_{SV40}-SEAP-pA Constitutive SEAP expressing vector	Clontech
pSO3	$P_{INF\text{-}\beta(ACD)}$-SEAP-pA SEAP expressing plasmid in pSEAP2	S. Österle (16, 63)
pSO4	P_{CMV}-DGCL-pA Light-dependent DGC expressing plasmid in pMM001;	S. Österle (16, 63)
pZKY121	P_{SV40}-DGCAwt-pA DGC expressing plasmid in pSBC-2	K. Zwicky (30, 61)
pZKY113	P_{SV40}-DGCL-pA Light-dependent DGC expressing plasmid in pSBC-2 P_{SV40}-DGC_light-pA	K. Zwicky (30, 61)
pSTING	P_{CMV}-STING-pA in pCMV-Sport6 backbone	Source Bioscience

Table 6. Plasmids used in the study

4.1.7 Implant parts and materials

Material/Part	Product ID	Manufacturer/Retailer

Glues/insulators		
EPOTEK 301 medical two-part epoxy glue	301-2FL-T	Epoxy Technology
Pattex PXP06 hot melt adhesive	245259 - 62	Conrad
Urethan 71	Art.Nr. 110-40-714	Distrelec
UHU Sekundenkleber	Bestell-Nr.: 053710 - 62	Conrad
Cell carriers		
Cytodex 1	CAS Number 79920-52-8	Sigma-Aldrich
Cytodex 3	CAS Number 88895-19-6	Sigma-Aldrich
Wires		
Mayerhofer Modellbau superthin copper wire 0.15mm	Bestell-Nr.: 242534 - 62	Conrad
Lacquered copper wire, 0.3mm	Bestell-Nr.: 605426 – 62	Conrad
Lacquered copper wire, 0.5mm	Bestell-Nr.: 605544 - 62	Conrad
Lacquered copper wire, 0.8mm	Bestell-Nr.: 605604 - 62	Conrad
Lacquered copper wire, 1mm	Bestell-Nr.: 605660 - 62	Conrad
Schaltdraht YV 1 x 0.2mm	Bestell-Nr.: 1180528 - 62	Conrad
LEDs		
LED690-03AU	-	Roithner Lasertechnik
L690-33AU	-	Roithner Lasertechnik
SMC700	-	Roithner Lasertechnik
3D printing materials		
PA 2200	-	3Dprintfabriek's Hub, at 3D Hubs
PLA	-	3DWelt's Hub, at 3D Hubs
ABS	-	3DWelt's Hub, at 3D Hubs
Formlabs standard resin	-	3dConception's Hub, at 3D Hubs
Microscrews		
M0.6 x 6 Brass Hex Bolt	-	Prime-Miniatures
M0.6 Open Hex Solid Brass	-	Prime-Miniatures
M0.6 Solid Brass Washers	-	Prime-Miniatures
Switches		
B3U-3000P, Omron	Art.Nr. 135-59-036	Distrelec
B3U-1000P, Omron	Art.Nr. 135-59-010	Distrelec
Drucktaster 12 V/DC 0.05 1	Bestell-Nr: 711746 - 62	Conrad
Drucktaster 12 V/DC 0.05 2	Bestell-Nr.: 711761 - 62	Conrad
Drucktaster 12 V/DC 0.05 3	Bestell-Nr.: 711700 – 62	Conrad
Membranes		
77 μm polyester mesh membrane	-	Reichelt Chemietechnik GmbH & Co
Polyethersulfonate membrane	PES452005	Sterlitech
Natureflex 42	-	Innovia

Table 7. Parts and materials used for cellulase sensor and implant engineering

4.2 Molecular biology methods

PCR

Q5 DNA polymerase was used to construct lentiviral vectors pMFl8…pMFl15, according to manufacturer's protocol. Taq polymerase was used for routine PCRs for construct verification, according to manufacturer's protocol.

Gel electrophoresis

For gel electrophoresis, 1% agarose gels containing 8 µl of RedSafe per 50 mL gel were used, at 80 V, 40 minutes, with GeneRuler Ladder as the reference. DNA was then visualized under 312 nm UV light or black light.

Electrocompetent cell preparation

E. coli seed cultures were prepared by inoculating 5 mL of LB from glycerol stocks and incubating overnight at 37°C, 400 rpm. 1 mL of culture was then inoculated to 80 mL of LB, incubated at 37°C, 400 rpm until OD_{600}=0.3..0.8. Cells were then centrifuged at 10000g, 10 min, 4 °C, washed twice with 10mL ice-cold dH_20, resuspended in 4ml of 4 °C 10% vol/vol glycerol, aliquoted to 50-100 µl aliquots and stored at -80 °C.

Plasmid DNA extraction

Plasmid DNA was extracted using ZR Plasmid Miniprep kits (miniprep), or JetStar 2.0 kits (midiprep) according to manufacturer's protocols.

Restriction enzyme digests and ligation

Appropriate restriction enzymes and 10X NEB CutSmart buffer were used according to NEB recommendations, with 0.5-3µg of DNA restricted using 1µl of each restriction enzyme in 20 µl reaction volumes. Digests were then heat inactivated according to NEB recommendations, purified using DNA Clean and Concentrator 5 PCR purification kit, and DNA ligated using T4 DNA ligase according to manufacturer's protocol at 15-25 °C overnight. In ligation reactions, 30 pMol backbone and 30-300 pMol of insert were commonly used.

Electroporation

Electrocompetent cells (50-100 µl) were thawed on ice for 5-15min, 1µl of DNA (50-500ng) was added and the bacteria electroporated at 1.8kV, 5ms, in an ice-cold 0.1cm GenePulser-cuvette. Bacteria were resuspended in 800 µl LB or SOC, grown for 1h at 37°C, 400 rpm in 15 mL Falcon tubes. Tubes were then centrifuged for 3 min, 10000g, 600µl of the media removed, and cells resuspended and plated onto LB-agar containing appropriate antibiotics. Plates were then incubated overnight at 37°C.

4.3 Cell culture

All cell lines were handled and subcultured according to distributor's instructions. Freezer stocks of cells were prepared by resuspending 1-2*10^6 cells in 1ml culture medium containing 10% DMSO, frozen at -80°C and transferred to -140 °C for long-term storage.

4.4 Transfection

HEK293T cells were cultured in DMEM (Gibco) with 10%FBS (Sigma) and 1% PenStrep (Gibco), and subcultured according to ATCC recommendations. For transfection, HEK293T cells were seeded at 20x10^5 cells per 10mm diameter dish (Corning) or at similar cell to area ratios on 6 – 96 well plates (see Table 7). Cells were transfected 24h after seeding with a 2µg:6µg/mL DNA:PEI solution, and incubated 8-16 hours at 37°C before media exchange with fresh DMEM-FBS-PenStrep. DNA-PEI transfection mix was prepared by adding DNA to appropriate volumes of DMEM without FBS or PenStrep, adding appropriate volume of PEI with immediate mixing, and incubating for 30 min at 37°C. before adding the mix to previously seeded cells. All transfections and tests were carried out with N=3 replicates, unless otherwise stated.

Transfection indications (HEK293T, hMSC-tert)				
Plate	**DNA (ng)**	**medium (uL)**	**medium (after DNA:PEI solution addition)**	**Cell seeding density**

10cm dish	20000	4000	8000	2.0E+06
6 well	4000	1000	2000	4.0E+05
12 well	2000	400	800	1.6E+05
24 well	1000	200		8.0E+04
48 well	500	100	200	4.0E+04
96 well	250	50	100	2.0E+04

Table 7. Transfection specifications

4.5 Near infrared inducible system

Cells transfected with NIR inducible system (pKZY113 or pSO4, pSTING and pSO3) were induced either using plate LEDs, single LEDs, or single LEDs powered wirelessly. For Plate LED induction, cells were seeded on 6 – 96 well plates, placed under plate LED at approximately 10 cm distance, and induced with NIR light at 50 mA for 0.5-16 hours. For single LED induction, single LEDs were connected to the LED driver and either placed over a well or glued to the membrane-covered cell chamber of the implant (using either EPO-TEK 301 medical glue, or Pattex hot melt adhesive) in sterile conditions. Cells previously transfected with the NIR inducible system and seeded on cytodex1 or cytodex 3 were then loaded into the implant, placed in 7 mL DMEM-10% FBS-1% PenStrep containing 10 μM biliverdin hydrochloride in 6 well plate wells, and induced with NIR light for 3-16 hours at 10-50 mA. SEAP was measured 24-96 hours later.

For single LEDs powered wirelessly, LEDs were soldered to wirelessly-powered RFID chip, attached to the cell chamber of the implant in sterile conditions, and RFID placed on active field generator, 3.3cm away from the surface (on top of two plastic Petri dishes) to induce cells with NIR light. Field generator was kept at room temperature, and at least 10 cm away in all directions from any other metallic objects during operation, to prevent overload-induced burnout.

For seeding cells on cytodex1 or cytodex 3, media was exchanged for DMEM-10% FBS-1% PenStrep after transfection, cells incubated for 6-16 hours, trypsinized, resuspended in fresh DMEM-10%FBS-1% PenStrep containing 10μM biliverdin hydrochloride, and seeded onto cytodex at $10*10^5$ cells/100 μL cytodex in non-coated 10cm dishes or 6-96 well plates. Cell-cytodex mix was then incubated for 6-24 hours to allow cell attachment, centrifuged at 500g, 2 min, washed with 10-20 mL of DMEM-10%FBS-1% PenStrep, centrifuged again, and resuspended in DMEM-10%FBS-1% PenStrep containing 10μM biliverdin hydrochloride, to a volume of the originally added cytodex (e.g. if 1 mL cytodex was added originally, cells were resuspended to a final volume of 1 mL). Implants were then loaded with 150-400 μL of cytodex, and sealed with a 200 μL pipette tips, with previously heat-sealed front ends to prevent leakage. SEAP was then measured 24-96 hours after induction.

4.6 Reporter assays

SEAP assay

1-5 days after induction, 10-80μl of samples were transferred to a 96 well plate, filled to 80μl with ddH_2O and heat inactivated at 65°C for 15-30 minutes and placed on ice. 20μl 120mM pNPP and 100μl 2X SEAP buffer were mixed and added to each well. The plate was then shaken at 800rpm for 15s and absorbance measured at 405nm at 37°C every 20 sec for a total of 30 times. SEAP concentration was then calculated from the determined slope, using Beer-Lambert law:

$$EA = 10^6 \cdot \frac{E}{a \cdot d} \cdot v \quad (1)$$

EA: Enzymatic activity [U/L]

c: Concentration increase [mol/(L min)]

E: Slope [min^{-1}]

v: Dilution factor [total assay volume/supernatant volume];

a: Molar extinction coefficient [18 600 mol/(L cm)];

d: Light traveling distance: 0.6 cm;

Cellulase assay

1-5 days after induction, 30µl of sample was transferred to 96-well plate wells. For each sample, 3µl of 10X Resofurin cellobioside (reaction substrate) was diluted in 27µl of Reaction Buffer, and mixture added to sample on ice. Fluorescence at excitation/emission of 570/585nm was then measured for 15-30 times with 2 min intervals at 37°C using a plate reader to determine the slope. The cellulase concentration was then interpolated from a previously determined standard curve, according to the equation below:

$$c = \frac{E - 8.649}{303.5} \quad (2)$$

c: Cellulase concentration (U/L)

E: Slope [min^{-1}]

4.7 Engineering cellulose-based cell-machine interface

Natureflex 42 were used as cellulose sheets for testing (Innovia). For testing of direct current (DC) based systems, 8ml of 1X PBS was pipetted into 4 layers of white kitchen roll tissue paper (3cm^2). These were then placed on either side of either a single cellulose sheet, cellulose covered with mineral oil (M5904, Sigma), or cellulose-mineral oil-cellulose, and connected to plate electrodes. Resistance of the circuit was then measured using NI miDAQ data acquisition device (National Instruments) at the 2-20kΩ range setting, and values recorded 2 seconds after start of measurement. To test the effect of membrane damage, resistance was measured before and after cutting a 2.2 cm diameter hole into the membrane.

For alternative current (AC) measurements, custom-made electrodes were prepared out of 2 mL spectrophotometry cuvettes (Sigma), 1.1mm diameter copper wire (Schaltdraht YV, Conrad) and hot-melt adhesive (Pattex). Cellulose sheet was attached between two parts with hot-melt adhesive glue, and electrolyte solution loaded into each part via loading ports at the top of the part (Fig. 2). AC was then applied in a sinusoid or discrete waveform, with V_{max}=1V, between 1Hz to 1kHz using NI USB 6008 data acquisition device (National Instruments). Data was acquired at 10x higher frequency than AC frequency using NI USB6008 and NI myDAQ and a custom-written program in LabView 2014 (National Instruments). Tests were run between 3 hours and 4 days, depending on experimental requirements. Due to the high volume of data generated per run (up to 30Gb), custom software was written in Python to down-sample and analyse data (AC_reduce_analyse.py, see Appendix). 1X PBS (Sigma) was used as electrolyte solution, and for cellulase degradation tests, *T. reesei* cellulase (liquid, Sigma) was used at 10% concentration (approximately 70U/ml). Degradation of cellulose membrane was visually confirmed after end of measurements.

For cellulose-printed resistor circuits, Ti/Au resistors of approximately 2Ω resistance was printed onto cellulose (prepared by Giovanni Salvatore, ETH Zurich – see Fig. 3A). Circuits were then wired by applying conductive glue (Wire Glue, AP) to a copper wire and wiring pad, and allowing to air-dry and solidify at 23 °C for 4-16 hours. 10% cellulase-PBS solution was then applied as a single 100µl drop, by complete submersion of resistor, or by exposing only the cellulose side of the resistor to solution (Fig. 3C). For drop and complete immersion, cellulose-resistors were taped at the edges onto glass slides for mechanical stability before applying the solution. For cellulose-exposure only (Fig. 3Cb), cellulose-resistors were first placed onto stick aluminium foil, with a 0.5x0.5cm hole to allow access to cellulase solution. The circuit side was then padded with 4 layers of parafilm (Demis) and taped onto a glass slide for mechanical stability. A small well made of a 1.5mL centrifuge tube was then glued above hole in aluminium foil, and cellulase solution (800 uL) added to the well. The well was then covered gently with parafilm and tape to reduce evaporation. Tests were carried out at 37°C and data acquired and analysed as for previous AC measurements.

For cellulose-wire systems, a 0.15mm diameter copper wire (Mayerhofer Modellbau, Conrad) was attached onto a 1.5x4cm cellulose sheet via superglue (UHU Sekundenkleber, Conrad). Small holes were then made at the ends of cellulose sheets to attach the sheet-wire onto a metal scaffold, using a 10mm diameter screw (Fig. 4A). The metal scaffold was folded from a 2cm wide metal sheet, to provide longitudinal tension. The system was then connected to NI miDaq and NI USB6008, device placed into PBS or PBS-cellulase solution, and current recorded at 1kHz 1V AC.

For cellulose-switch systems (the design ultimately used in the implant), 5 different microswitches (see Table 7) were tested for their mechanical, size, and robustness compatibility w.r.t operating in a small compartment in aqueous solutions, and PCB Switch side actuated was chosen as the best-performing and most suitably sized switch. To create the cellulose-switch system, a switch port was designed and 3D printed over successful design-build-test cycles to house the switch. To build the cellulose-switch system, the microswitch was placed in the switch port, covered with a 1-3 fold Natureflex 42 sheet, attached with microscrews, and tensioned to turn on the switch, by screwing the microscrews at the backside of the port. Operation of the cellulose-switch system was then tested in PBS, DMEM or cell culture with or without purified cellulase (see Results section for details), and current recorded as described above.

4.8 Implant design, engineering and 3D printing

All designs for 3D printing were made using Blender (Blender Foundation), and designs rendered using Cura (Ultimaker). For prototyping, designs were printed from PLA using Ultimaker or Ultimaker^2 3D printers (Ultimaker) from a 3 mm standard white PLA filament. Printing parameters were extensively varied to increase printing resolution: PLA was commonly printed at temperatures between 180-220°C, 90-140% extrusion compensation, 80% fill density, no base plate heating, 20mm/s speed, 0.06mm layer height, 0.4mm nozzle diameter, 20% fill rate, 60% initial plate diameter, 100% fan speed. For more detailed parts, which exceeded the resolution of Ultimaker or Ultimaker2, parts were ordered from 3D Hubs, from 3Dprintfabriek's Hub and 3DConception's Hub for printing with PA 2200 or Standard Formlabs resin respectively.

The implant cell chamber was constructed by applying mixed Epotek 301 glue onto both sides of the 3D printed cell chamber, and placing porous membranes of polyethersulfonate with 450 μm pore size (inner membrane), and 77 μm monofilament polyester mesh (outer reinforcement membrane). The glue was then cured at 40°C for 4 hours or 60°C for 2-3 hours. After curing, cell chamber was visually inspected and any holes or insufficiently glued areas filled again with either Epotek 301 glue or by Pattex hot melt adhesive. The cell chamber, as well as LED and/or microswitch (the latter soldered to the RFID chip) and the implant encasings were then sterilized with 70% ethanol and 1h UV light exposure. Before attachment to the cell chamber, the RFID chip (but not LED and microswitch) was first insulated by applying Epotek 301 glue or spray-on Urethane 71, to remove the possibility of water damage to the chip. The implant was then assembled in a sterile environment using Epotek 301, cured and inspected for any irregularities.

V References

1. Pardee K, et al. (2014) Paper-Based Synthetic Gene Networks. *Cell* 159(4):940–954.
2. Webb AJ, et al. (2016) A protease-based biosensor for the detection of schistosome cercariae. *Sci Rep* 6:24725.
3. Diesel E, Schreiber M, van der Meer JR (2009) Development of bacteria-based bioassays for arsenic detection in natural waters. *Anal Bioanal Chem* 394(3):687–93.
4. Gu MB, Mitchell RJ, Kim BC (2004) Whole-cell-based biosensors for environmental biomonitoring and application. *Adv Biochem Eng Biotechnol* 87:269–305.
5. Gopal K V Neurotoxic effects of mercury on auditory cortex networks growing on microelectrode arrays: a preliminary analysis. *Neurotoxicol Teratol* 25(1):69–76.
6. Liu Q, et al. (2014) Cell-Based Biosensors and Their Application in Biomedicine. *Chem Rev* 114(12):6423–6461.
7. Kemmer C, et al. (2010) Self-sufficient control of urate homeostasis in mice by a synthetic circuit. *Nat*

Biotechnol 28(4):355–60.

8. Schukur L, Geering B, Charpin-El Hamri G, Fussenegger M (2015) Implantable synthetic cytokine converter cells with AND-gate logic treat experimental psoriasis. *Sci Transl Med* 7(318):318ra201-318ra201.

9. Weber W, Fussenegger M (2012) Emerging biomedical applications of synthetic biology. *Nat Rev Genet* 13(1):21–35.

10. Ye H, Aubel D, Fussenegger M (2013) Synthetic mammalian gene circuits for biomedical applications. *Curr Opin Chem Biol* 17(6):910–917.

11. Kemmer C, et al. (2011) A designer network coordinating bovine artificial insemination by ovulation-triggered release of implanted sperms. *J Control Release* 150(1):23–9.

12. Orive G, et al. (2003) Cell encapsulation: promise and progress. *Nat Med* 9(1):104–7.

13. Orive G, et al. (2015) Cell encapsulation: technical and clinical advances. *Trends Pharmacol Sci* 36(8):537–46.

14. Lathuilière A, Cosson S, Lutolf MP, Schneider BL, Aebischer P (2014) A high-capacity cell macroencapsulation system supporting the long-term survival of genetically engineered allogeneic cells. *Biomaterials* 35(2):779–91.

15. Lathuilière A, et al. (2014) Genetic engineering of cell lines using lentiviral vectors to achieve antibody secretion following encapsulated implantation. *Biomaterials* 35(2):792–802.

16. Folcher M, et al. (2014) Mind-controlled transgene expression by a wireless-powered optogenetic designer cell implant. *Nat Commun* 5:5392.

17. Lathuilière A, Schneider BL (2016) Lentiviral Vectors for the Engineering of Implantable Cells Secreting Recombinant Antibodies, pp 139–155.

18. Eriksdotter-Jönhagen M, et al. (2012) Encapsulated cell biodelivery of nerve growth factor to the Basal forebrain in patients with Alzheimer's disease. *Dement Geriatr Cogn Disord* 33(1):18–28.

19. Ye H, Daoud-El Baba M, Peng R-W, Fussenegger M (2011) A synthetic optogenetic transcription device enhances blood-glucose homeostasis in mice. *Science* 332(6037):1565–8.

20. Müller K, Weber W (2013) Optogenetic tools for mammalian systems. *Mol Biosyst* 9(4):596–608.

21. Leung DW, Otomo C, Chory J, Rosen MK (2008) Genetically encoded photoswitching of actin assembly through the Cdc42-WASP-Arp2/3 complex pathway. *Proc Natl Acad Sci* 105(35):12797–12802.

22. Ryu M-H, Gomelsky M (2014) Near-infrared Light Responsive Synthetic c-di-GMP Module for Optogenetic Applications. *ACS Synth Biol* 3(11):802–810.

23. Ryu M-H, et al. (2014) Engineering adenylate cyclases regulated by near-infrared window light. *Proc Natl Acad Sci* 111(28):10167–10172.

24. Tarutina M, Ryjenkov DA, Gomelsky M (2006) An unorthodox bacteriophytochrome from Rhodobacter sphaeroides involved in turnover of the second messenger c-di-GMP. *J Biol Chem* 281(46):34751–8.

25. Sun L, et al. (2013) Cyclic GMP-AMP synthase is a cytosolic DNA sensor that activates the type I interferon pathway. *Science* 339(6121):786–91.

26. Katritch V, Cherezov V, Stevens RC (2013) Structure-Function of the G Protein–Coupled Receptor Superfamily. *Annu Rev Pharmacol Toxicol* 53(1):531–556.

27. Rosenbaum DM, Rasmussen SGF, Kobilka BK (2009) The structure and function of G-protein-coupled receptors. *Nature* 459(7245):356–363.

28. Heng BC, Aubel D, Fussenegger M (2014) G protein-coupled receptors revisited: therapeutic applications inspired by synthetic biology. *Annu Rev Pharmacol Toxicol* 54:227–49.

29. Heifetz A, et al. (2015) GPCR structure, function, drug discovery and crystallography: report from Academia-Industry International Conference (UK Royal Society) Chicheley Hall, 1-2 September 2014. *Naunyn Schmiedebergs Arch Pharmacol* 388(8):883–903.

30. Ye H, et al. (2013) Pharmaceutically controlled designer circuit for the treatment of the metabolic syndrome. *Proc Natl Acad Sci U S A* 110(1):141–6.

31. Peng W, et al. (2010) Transduction of tumor-specific T cells with CXCR2 chemokine receptor improves migration to tumor and antitumor immune responses. *Clin Cancer Res* 16(22):5458–68.

32. Wu C-Y, Rupp LJ, Roybal KT, Lim WA (2015) Synthetic biology approaches to engineer T cells. *Curr Opin Immunol* 35:123–130.

33. Mukherjee K, Bhattacharyya S, Peralta-Yahya P (2015) GPCR-Based Chemical Biosensors for Medium-Chain Fatty Acids. *ACS Synth Biol* 4(12):1261–1269.

34. Crawford RL (1981) *Lignin Biodegradation and Transformation* (John Wiley & Sons, New York, New York, USA).

35. Kalia S, et al. (2011) Cellulose-Based Bio- and Nanocomposites: A Review. *Int J Polym Sci* 2011:1–35.

36. Lee K-Y, Buldum G, Mantalaris A, Bismarck A (2014) More than meets the eye in bacterial cellulose: biosynthesis, bioprocessing, and applications in advanced fiber composites. *Macromol Biosci* 14(1):10–32.

37. Kemmer C, et al. (2011) A designer network coordinating bovine artificial insemination by ovulation-triggered release of implanted sperms. *J Control Release* 150(1):23–29.

38. Fjord-Larsen L, et al. (2010) Long-term delivery of nerve growth factor by encapsulated cell biodelivery in the Göttingen minipig basal forebrain. *Mol Ther* 18(12):2164–72.

39. Goren A, Dahan N, Goren E, Baruch L, Machluf M (2010) Encapsulated human mesenchymal stem cells: a unique hypoimmunogenic platform for long-term cellular therapy. *FASEB J* 24(1):22–31.

40. Wallrapp C, et al. (2013) Cell-based delivery of glucagon-like peptide-1 using encapsulated mesenchymal stem cells. *J Microencapsul* 30(4):315–324.

41. Cierpka K, et al. (2013) hMSC Production in Disposable Bioreactors with Regards to GMP and PAT. *Chemie Ing Tech* 85(1–2):67–75.

42. Thumann G, et al. (2010) High efficiency non-viral transfection of retinal and iris pigment epithelial cells with pigment epithelium-derived factor. *Gene Ther* 17(2):181–189.

43. Wu L, Pan Y, Chen G-Q, Matsunami H, Zhuang H (2012) Receptor-transporting protein 1 short (RTP1S) mediates translocation and activation of odorant receptors by acting through multiple steps. *J Biol Chem* 287(26):22287–94.

44. Saito H, et al. (2004) RTP Family Members Induce Functional Expression of Mammalian Odorant Receptors. *Cell* 119(5):679–691.

45. Pham DH, Moretti PAB, Goodall GJ, Pitson SM (2008) Attenuation of leakiness in doxycycline-inducible expression via incorporation of 3’ AU-rich mRNA destabilizing elements. *Biotechniques* 45(2):155–6, 158, 160 passim.

46. Takata Y, Kondo S, Goda N, Kanegae Y, Saito I (2011) Comparison of efficiency between FLPe and Cre for recombinase-mediated cassette exchange in vitro and in adenovirus vector production. *Genes Cells* 16(7):765–77.

47. Sanjana NE, Shalem O, Zhang F (2014) Improved vectors and genome-wide libraries for CRISPR screening. *Nat Methods* 11(8):783–784.

48. Valva P, Ríos DA, De Matteo E, Preciado M V (2016) Chronic hepatitis C virus infection: Serum biomarkers in predicting liver damage. *World J Gastroenterol* 22(4):1367–81.

49. Ciborowski P (2009) Biomarkers of HIV-1-associated neurocognitive disorders: challenges of proteomic approaches. *Biomark Med* 3(6):771–85.

50. Hurst J, et al. (2015) Immunological biomarkers predict HIV-1 viral rebound after treatment interruption. *Nat Commun* 6:8495.

51. Duffy M., et al. (2003) Clinical utility of biochemical markers in colorectal cancer. *Eur J Cancer* 39(6):718–727.

52. Maussier ML, Valenza V, Schinco G, Galli G AFP, CEA, CA 19-9 and TPA in hepatocellular carcinoma. *Int J Biol Markers* 5(3):121–6.

53. Gish RG (2014) Early detection of hepatocellular carcinoma through surveillance using biomarkers. *Gastroenterol Hepatol (N Y)* 10(2):121–3.

54. Prensner JR, Rubin MA, Wei JT, Chinnaiyan AM (2012) Beyond PSA: the next generation of prostate cancer biomarkers. *Sci Transl Med* 4(127):127rv3.

55. Locker GY, et al. (2006) ASCO 2006 Update of Recommendations for the Use of Tumor Markers in Gastrointestinal Cancer. *J Clin Oncol* 24(33):5313–5327.

56. Babuin L, Jaffe AS (2005) Troponin: the biomarker of choice for the detection of cardiac injury. *CMAJ* 173(10):1191–202.

57. Sugita T, et al. (2015) Analysis of the Serum Bile Acid Composition for Differential Diagnosis in Patients with Liver Disease. *Gastroenterol Res Pract* 2015:1–10.

58. Jahnel J, et al. (2015) Serum Bile Acid Levels in Children With Nonalcoholic Fatty Liver Disease. *J Pediatr Gastroenterol Nutr* 61(1):85–90.

59. Adipietro KA, et al. (2012) Functional Evolution of Mammalian Odorant Receptors. *PLoS Genet* 8(7):e1002821.

60. Locher S (2011) Master Thesis: A perfume match maker olfactory binding protein as active filter for olfactory receptor.

61. Zwicky K (2011) Master Thesis: Design of an orthogonal synthetic gene regulation network in eukaryotes, 2011.

62. Weber W, et al. (2002) Versatile macrolide-responsive mammalian expression vectors for multiregulated multigene metabolic engineering. *Biotechnol Bioeng* 80(6):691–705.

63. Österle S (2012) Master Thesis: A biocybernetic interface linking the human mind to gene expression.

Acknowledgements

I would like to thank Marc Folcher for his valuable advice, guidance, support, interesting discussions and ideas through the entire work. I would also like to thank Prof. Dr. Martin Fussenegger for being welcoming, and for the opportunity to join his diverse group.

Furthermore, I would like to thank Giovanni Salvatore for making the cellulose resistors and Peter Buchmann for making the RFID chip and field generator and for advice and discussions throughout the project.

Finally I would like to thank Babak Nichabouri for his initial support and guidance, Damian Hausherr for being a dependable lab partner, Marius Müller, Helene Chassin, Leo Schneller and Victor Hällman for sharing plasmids and ideas, and all the members in the Fussenegger group for making this a great experience.

Appendix

Programs

1 AC_reduce_analyse.py

#This program takes current measurements generated by NI Labview, downsamples them by saving datapoints #every n seconds, converts them to root mean squared, saves downsampled and analysed data in a new file, and #plots the output

```
from openpyxl import Workbook
from openpyxl.compat import range
from openpyxl.cell import get_column_letter
import math
import sys
inputfile = open('inputfile', 'r')
outputfile = open('outputfile', 'w')
averagingtime=2 #averaging time in seconds
timeinterval = 120
samplingrate= 1000
counter=0
for line in inputfile:
        newlines=line.split(",")
        if counter<=(averagingtime*samplingrate+23):
                outputfile.write(line)
                counter=counter+1
        if (averagingtime*samplingrate+23)<=counter and counter<(samplingrate*timeinterval+23):
                counter=counter+1
        if counter==(samplingrate*timeinterval+23):
                counter=0

inputfile.close()
outputfile.close()

from openpyxl import Workbook
from openpyxl.compat import range
from openpyxl.cell import get_column_letter
import math
import sys

inputfile = open('input', 'r')
outputfile = open('output', 'w')
averagingtime=1 #aveaging time in seconds
timevalue = 1
samplingrate= 1000
whichline=2
data = inputfile.readlines()
output = []
output2=[]
output3=[]
output4=[]
time = []
i = 0
for i in range(len(data)):
   line = data[i]
   line=line.split(',')
   if i >22:
        #Record time
        timevalue2=str(line[0])
```

```
            timevalue2=timevalue2.rstrip()
            time.append(timevalue2)

            #Record measurements
            outputvalue=str(line[whichline])
            outputvalue=outputvalue.rstrip()
        output.append(outputvalue)

#value of time over which mean values are averaged
RMS=[]
samplenumber=0
samplenumber=timevalue*samplingrate #determines the no of samples over which RMS is taken
print samplenumber, timevalue, samplingrate
samplenumber=int(samplenumber)
print samplenumber
meanvalue=0
meanvalue=float(meanvalue)
#
RMStime=[]
counter=0
for i in range(len(output)):
            if counter<samplenumber:
                        meanvalue=meanvalue+(float(output[i])*float(output[i]))
                        counter=counter+1
            if counter==samplenumber:
                        meanvalue=meanvalue+(float(output[i])*float(output[i]))
                        meanvalue=math.sqrt(meanvalue/samplenumber)
                        RMS.append(meanvalue)
                        RMStime.append(float(time[i])/60)
                        meanvalue=0
                        counter=0
            if counter>samplenumber:
                        sys.exit("Error message")
print RMStime

#Choosing the final datapoints which to show and write - here
RMSfinal=[]
RMStimefinal=[]
nthsample=float(averagingtime)/(float(timevalue))
nthsample=int(nthsample)
for i in range(0, len(RMS), nthsample):
            RMSfinal.append(RMS[i])
            RMStimefinal.append(RMStime[i])

#print RMSfinal
print RMStimefinal

#sample rates
#write RMS values to a file
for i in range(len(RMSfinal)):
            outputfile.write(str(RMStimefinal[i])+' ')
            outputfile.write(str(RMSfinal[i])+'\n')
outputfile.close()

#plot
import matplotlib.pyplot as plt
```

```
plt.plot(RMStimefinal,RMSfinal)
plt.ylabel('Ampers')
plt.xlabel('Time(min)')
plt.show()
```